Computational and Structural Biotechnology Journal 19 (2021) 1214–1232

COMPUTATIONAL AND STRUCTURAL BIOTECHNOLOGY JOURNAL

journal homepage: www.elsevier.com/locate/csbj

Biochemical and Structural Characterization of a novel thermophilic esterase EstD11 provide catalytic insights for the HSL family

Vega Miguel-Ruano [a,3], Ivanna Rivera [a,3], Jelena Rajkovic [b,3], Kamila Knapik [c], Ana Torrado [b], José Manuel Otero [d,1], Elisa Beneventi [d,2], Manuel Becerra [c], Mercedes Sánchez-Costa [e], Aurelio Hidalgo [e], José Berenguer [e], María-Isabel González-Siso [c], Jacobo Cruces [d], María L. Rúa [b,*], Juan A. Hermoso [a,*]

[a] Department of Crystallography and Structural Biology, Institute of Physical-Chemistry "Rocasolano", Spanish National Research Council (CSIC), Madrid, Spain
[b] Biochemistry Laboratory, CITACA-Agri-Food Research and Transfer Cluster, Campus Auga, University of Vigo, Ourense, Spain
[c] EXPRELA Group, University A Coruña, Science Faculty, Advanced Scientific Research Center (CICA), A Coruña, Spain
[d] GalChimia, S.A., Cebreiro, A Coruña, Spain
[e] Department of Molecular Biology, Center for Molecular Biology "Severo Ochoa" (UAM-CSIC), Autonomous University of Madrid, Madrid, Spain

ARTICLE INFO

Article history:
Received 6 November 2020
Received in revised form 27 January 2021
Accepted 30 January 2021
Available online 10 February 2021

Keywords:
Crystal structure
Metagenomic
Thermophilic esterase
α/β hydrolase fold
Enzyme-substrate complex

ABSTRACT

A novel esterase, EstD11, has been discovered in a hot spring metagenomic library. It is a thermophilic and thermostable esterase with an optimum temperature of 60°C. A detailed substrate preference analysis of EstD11 was done using a library of chromogenic ester substrate that revealed the broad substrate specificity of EstD11 with significant measurable activity against 16 substrates with varied chain length, steric hindrance, aromaticity and flexibility of the linker between the carboxyl and the alcohol moiety of the ester. The tridimensional structures of EstD11 and the inactive mutant have been determined at atomic resolutions. Structural and bioinformatic analysis, confirm that EstD11 belongs to the family IV, the hormone-sensitive lipase (HSL) family, from the α/β-hydrolase superfamily. The canonical α/β-hydrolase domain is completed by a cap domain, composed by two subdomains that can unmask of the active site to allow the substrate to enter. Eight crystallographic complexes were solved with different substrates and reaction products that allowed identification of the hot-spots in the active site underlying the specificity of the protein. Crystallization and/or incubation of EstD11 at high temperature provided unique information on cap dynamics and a first glimpse of enzymatic activity *in vivo*. Very interestingly, we have discovered a unique Met zipper lining the active site and the cap domains that could be essential in pivotal aspects as thermo-stability and substrate promiscuity in EstD11.

1. Introduction

Carboxylesterases (carboxylester hydrolases, E.C. 3.1.1.1) and lipases (triacylglycerol acylhydrolases, E.C. 3.1.1.3) from microbial origin have increasingly gained interest in research, and a considerable number of novel enzymes have been discovered and characterized. In spite of their similar secondary structures, i.e., both class of enzymes are members of the α/β-hydrolase fold enzyme superfamily, one of the largest groups of structurally related enzymes, and bear a catalytic triad formed by Ser-Asp/Glu-His, they differ in substrate specificity [1,2]. In a broad sense, esterases show preference for short-chain (<10–12 carbon atoms) water-soluble fatty acid esters and lipases do so for water-insoluble long-chain (greater than 10–12 carbon atoms) [3,4]. Esterases and lipases count with the largest number of industrial applications as they

Abbreviations: HSL, hormone-sensitive lipase; *p*NP, 4-nitrophenol; CHCA, cyclohexane carboxylic acid; NP, naproxen; MNP, methyl-naproxen; FLU, fluorescein; DMSO, dimethyl sulfoxide; PPL, Porcine Pancreatic Lipase; CV, column volume; LDAO, N,N-dimethyldodecylamine N-oxide; CMC, critical micellar concentration; DSF, Differential scanning fluorimetry.

* Corresponding authors.
E-mail addresses: vmruano@iqfr.csic.es (V. Miguel-Ruano), ivannaiq@gmail.com (I. Rivera), rajkovic.j@gmail.com (J. Rajkovic), kamila.knapik@gmail.com (K. Knapik), agrasar@uvigo.es (A. Torrado), jose.otero@usc.es (J.M. Otero), Elisa.Beneventi@rd.nestle.com (E. Beneventi), manuel.becerra@udc.es (M. Becerra), mercedes.sanchez@cbm.csic.es (M. Sánchez-Costa), ahidalgo@cbm.csic.es (A. Hidalgo), jberenguer@cbm.csic.es (J. Berenguer), isabel.gsiso@udc.es (M.-I. González-Siso), jacobo.cruces@galchimia.com (J. Cruces), mlrua@uvigo.es (M.L. Rúa), xjuan@iqfr.csic.es (J.A. Hermoso).
[1] Current address: Research Facilities Area, Santiago de Compostela University, CACTUS bldg, Santiago de Compostela (A Coruña), Spain.
[2] Current address: Chemical Food Safety Group, Nestlé Research, Lausanne, Switzerland.
[3] Equally contributed authors.

https://doi.org/10.1016/j.csbj.2021.01.047

accept a broad range of non-natural substrates and can be used in a variety of reaction media including organic solvents [5]. Many of them show high regio- and stereoselectivity, as well as stability, in organic solvents. Frequently they also show "catalytic promiscuity", that is the enzyme's ability to catalyze more than one type of chemical transformation [6,7], such CAL-A from *Pseudozyma antarctica* [8,9] or Est8 that act as hydrolases but also show acyltransferase activity in water [7]. Their applications are wide in several fields, for example, food and paper industries, biodiesel fuel production, additive in detergents, synthesis of fine chemicals and optically pure compounds, degradation of pesticides in wastewater treatment, etc. [10]. Attempts to predict the substrate promiscuity level have been explored for several esterases deepen on their sequences and structural data [7,11].

Arpigny and Jaeger first classified the bacterial lipolytic enzymes (esterases and lipases) into eight families (I-VIII) with subfamilies, on the basis of their conserved amino acid sequences and their biological features [12]. The progressive discovery of new esterases, largely due to metagenomic approaches, expanded the original classification first to 15 families [8,13] that in recent reviews have been extended to 19 families and eight true lipase sub-families [14] and later to 35 families and 11 true lipase subfamilies [15].

The family IV consists of a group of lipolytic enzymes from distantly related prokaryotes including psychrophilic, mesophilic, and thermophilic which share sequence similarities with mammalian hormone-sensitive lipase (HSL) [6,14]. Apart from the characteristic GXSXG motif around the active site serine, which is also found in serine proteases, they contain a conserved HGGG consensus sequence upstream the catalytic site which participates in the oxyanion hole formation. The catalytic serine residue, along with an acidic residue (aspartate or glutamate) and a histidine, to which the acidic residue is hydrogen-bonded, form a highly conserved catalytic triad [16]. According to the sequence of the motif surrounding the catalytic serine residue, members of the HSL family are further divided into two subfamilies with GD**S**AG and GT**S**AG variants of this sequence [17,18]. In contrast to the enzymes belonging to GD**S**AG group, those from GT**S**AG group have been poorly characterized [19]. Esterases with a new variant of the conserved GXSXG motif with a Cys residue next to the catalytic Ser have been described within the HSL family [20].

A number of three-dimensional structures of HSLs have been published, including EstE2, EstE7, Est22 and Est25 from metagenomic libraries [21–23], Sto-Est from *Sulfolobus tokodaii* [24], PestE from the hyperthermophilic archaeon *Pyrobaculum calidifontis VA1* [25] or Brefeldin A Esterase (BFAE) from *Bacillus subtilis* [23]. Also, novel hydrolases, including carboxylesterases, have been discovered and characterized from hot and other extreme environments [26]. They have revealed that HSL typically is integrated by two domains, a CAP domain and a catalytic domain with a classical α/β-fold structure with a functional serine at the active site. The CAP domain consists of two N-terminal alpha helices and participates in substrate binding [27]. Most of bacterial HSLs have preference to hydrolyze short-chain *p*-nitrophenyl esters, tributyrin or vinyl propionate but show typical lipase kinetics [14] although HSLs are promiscuous by nature, and this has been related to their physiology, evolution, and metabolism [6]. HSL esterases have been recently review in Kim [6].

Metagenomics studies the set of genomes (metagenome) in an environmental microbial community. At present, this methodology is a valuable instrument for the exploration of enzyme biodiversity in nature, since the genomes of unculturable organisms, that could overcome 99% of total, are included in the metagenomes, thus allowing to unveil the enzymes of such organisms. Extremophilic microbial communities can provide enzymes with extreme pH and temperature working range, enhanced stability and other desired properties [13,28]. This opens a new horizon of enzymes with potentially novel and exclusive properties [29].

In this study, the thermal spring of Lobios (Ourense, Spain) was chosen to undertake the bioprospection of novel lipolytic enzymes. This is due to the high temperature (76°C) and alkaline pH (8.2) of this thermal source, pointing it out as a potential source of new thermostable and alkaline-tolerant industrial value enzymes. The objectives of this work were to isolate a novel lipolytic enzyme gene by functional metagenomics of this thermophilic environment, to over-express the gene yielding an active protein, and to characterize the produced protein in view of its biotechnological applications. Also, we intended the determination of the three-dimensional structure of the novel enzyme and the relationship of its structure with its function and biochemical characteristics. A novel lipolytic enzyme has been discovered that shows remarkable stability and performance on different reaction media and substrates with industrial interest, some of them synthesized ad hoc as models for this work, features that are supported by the structural determination here presented.

2. Materials and methods

2.1. Materials

The *p*NP derivatives butyrate, octanoate, decanoate, dodecanoate and tetradecanoate, hexaoctanoate, 3-[(3-Cholamidopropyl)-dimethylammonio]-1-propanesulphonate (CHAPS), cellosolve and fluorescein dilaurate were from Sigma Aldrich (St. Louis, MO, USA). Fluorescein dihexanoate and dioctanoate were synthesized by GalChimia, S.L., (O Pino, A Coruña, Spain, https://www.galchimia.com). Molecular weight markers for electrophoresis were obtained from Bio-Rad (Richmond, CA, USA). All other chemicals were of the purest grade available.

2.2. Methods

2.2.1. Sampling and DNA extraction

Water samples were collected from a hot spring in the Lobios municipality, situated on the shore of the Río Caldo river (GPS 41.86113, −8.1062), in the province of Ourense (Galician region, North-West of Spain). The thermal spring was located underground a Spa Hotel & Resort Balneario, with water temperature of 77°C and pH of 8.2. The sampling was performed on 14 January 2014. 125 L of water were collected into 5 sterile (ethanol prewashed) 25-liters plastic containers, using a hose connected to the pump hose system of the underground thermal spring. Samples were transported to the laboratory and processed the next day.

The hot spring water was vacuum filtered through 0.2-μm cellulose nitrate membranes (sterile, 47-mm diameter) to trap microbial cells on top of the filters, 2 membranes per each 25 L bottle were used, and high molecular weight (HMW) DNA was isolated (five extractions, one per 25-liters bottle) using the Epicentre Metagenomic DNA Isolation Kit for Water (Cat. No. MGD08420). DNA concentration was measured using NanoPhotometer, BioNova cientifica.

2.2.2. Metagenomic library construction

Metagenomic library was constructed using the CopyControl™ HTP Fosmid Library Production Kit with (Epicentre) according to the manufacturer's protocol with one modification: pCT3FK vector was used instead of pCC2FOS. The fosmid vector pCT3FK is a shuttle vector that can be used with either *E. coli* or *T. thermophilus* as the host [30]. DNA extracted from water was end-repaired and directly used for the ligation reaction.

Approximately 300 ng of DNA was ligated to 500 ng of the linearized fosmid pCT3FK vector, packaged into the lambda phage and used to infect *E. coli* EPI300-T1R cells. The library size (132,000 clones) was determined by dilution titering on LB (1% tryptone, 0.5% yeast extract, and 1% NaCl) agar plates containing 12.5 μg/ml chloramphenicol (LB/Cm). The resulting fosmid library was plated onto 91 LB/Cm plates at a density of ≈2000 bacterial clones per plate. Colonies from each plate were resuspended in 2.5 ml of LB containing 20% glycerol, and a 150 μl aliquot was transferred to a 96-well plate (3 identical 96-well plates were prepared). The library, named RCWL2, was stored at −80°C.

The average DNA insert size was estimated by isolation and purification of 20 randomly chosen fosmids. DNA mini-preparations were digested with BamHI. Insert size was determined using Bio-Rad software after electrophoresis on agarose gels. Size of the fosmid clones ranged from 24.5 kb to 50.1 kb, with average size of 35 kb.

2.2.3. Functional screening

For functional screening, the RCWL2 library was defrosted from −80°C freezer and 10–20 μl were transferred to a microtiter plate containing 130–140 μl of LB/Cm and cultured overnight at 37°C with shaking. RCWL2 library was then replicated onto LB plates containing 1% tributyrin using a 48-pin hand replicator. The plates were incubated at growth temperature (37°C) for 3 days, and then transferred to 65°C for 24 h to reveal the activity of the potential positive clones. Extended incubation times presumably lead to the stationary phase of the cultures that together with the incubation at 65°C might have promoted cell lysis, thus allowing the heterologous intracellular enzyme to contact the extracellular medium. Lipolytic activity was then identified by the formation of a clear halo resulting from the hydrolysis of tributyrin around the stamped colonies. This selection method is rather common to screen DNA libraries constructed in *E. coli* for detecting genes conferring lipolytic activity [31–33]. The clone that showed lipolytic activity was isolated by streak seeding on tributyrin plates in order to obtain single colonies surrounded by clear halos.

2.2.4. Sequence analysis

The fosmid DNA of the positive clone was amplified in *E. coli*, purified by using the FosmidMAX DNA purification kit (Epicentre Biotechnologies) and sequenced by massively parallel sequencing at Genoinseq (Cantanhede, Portugal). The library was prepared with the Nextera XT DNA Sample Preparation kit (Illumina) and sequenced using paired-end 2x300 bp on the MiSeq® Illumina® platform. The resulting reads were assembled with the SPAdes software (versión 3.7.1) after trimming low-quality bases and removing short reads (<100 bp). Low coverage and short contigs were removed to lead to the final sequence.

The open reading frame (ORF) encoding the putative esterase, named thereafter as EStD11was predicted using the ORF finder (https://www.ncbi.nlm.nih.gov/orffinder/). The similarity searches were carried out with BLASTP [34]. The amino acid sequence of the candidate identified lipolytic protein was aligned using Clustal Omega [35] with five top hits from BLASTP search together with 26 lipolytic enzymes sequences from previously established groups (I–VIII) [12]. The resulting alignment was used to construct the phylogenetic tree in MEGA7 [36] using a Poisson correction method, pairwise deletion of gaps and the neighbor-joining method with 1000 bootstrap replications. Physicochemical parameters of the protein were predicted by ProtParam online tool [37].

2.2.5. Molecular cloning and mutagenesis (UAM)

EstD11 gene was amplified by PCR using the Pfu Ultra II HS DNA polymerase (Agilent technologies) with oligonucleotides 5′-aaaaaacatatggcaagtgaagcactg −3′ and 5′-aaaaaagaattcttactgccaa tgctggc-3′ from the purified fosmid, and cloned into pET22 plasmid without other additional sequences using the restriction enzymes NdeI and EcoRI, which recognition sequences were included in the primers (underlined). EstD11 S144A catalytic mutant was generated in the expression plasmid using QuikChange™ (Stratagene, CA, USA) with oligonucleotides 5′-gccggccgcatcgccggcaatggc-3′ and 5′-gccattgccggcgatgcggccggc-3′.

2.2.6. Overexpression

The EstD11 gene was expressed in *E. coli* BL21(DE3). The recombinant bacteria was grown by incubation at 37 °C for 12 h in a rotary shaker at 150 rpm in 50 ml of LB medium (1% (w/v) peptone, 0.5% (w/v) yeast extract, 1% (w/v) NaCl, pH 7.2) with 100 μg/ml ampicillin. Cells were harvested and used as inoculum at an initial concentration of 1×10^6 UFC/ml for overexpression of the recombinant lipase in a 5 L BIOFLO III stirred-tank bioreactor (New Brunswick Scientific, USA), filled up with 4 L of LB plus 100 μg/ml ampicillin and incubated at 37°C, 300 rpm and an air flow rate of 0.5 (v/v). When OD_{600} reached 0.6 units (around two hours), 0.5 mM IPTG was added to induce expression. The culture progress was followed by biomass concentration and pO_2 measurement, and stopped when biomass just reached the plateau of the stationary phase (around 6 h after addition of IPTG) to avoid cell lysis. This moment coincided with an inflexion point on the pO_2, when it started to increase from the lowest level (below 5% O_2 saturation) reached at the end of the active growth phase. Expression started around one hour after induction and continued linearly until growth stopped, without appreciable extracellular enzyme. Cells were then collected, resuspended in 0.25 M sodium phosphate (pH 7.2), lysed by sonication, and the supernatant with the intracellular enzyme was finally recovered after centrifugation at 25,000 × *g* and 4°C for 15 min.

2.2.7. Downstream processing

Clear supernatant was subjected to thermal precipitation by incubating at 60°C for 15 min, followed by the centrifugation (10,000 × g, 4°C, 30 min). Subsequent chromatographic steps were run on ÄKTA Purifier 10 (GE Healthcare BioSciences AB, Uppsala, Sweden) at room temperature. Hydrophobic interaction chromatography (HIC) was run on a Butyl-Sepharose CL-4B column (2.6 cm × 8.5 cm, 45 ml CV) equilibrated with 0.25 M sodium phosphate buffer (pH 7.2). The column was washed at 0.7 ml min^{-1} with 6 CV of equilibration buffer, and eluted in two steps: (1) 13 CV decreasing the concentration of the elution buffer from 100% (equilibration buffer) to 1 mM sodium phosphate buffer (pH 7.2); (2) 2 CV with 1 mM sodium phosphate buffer (pH 7.2). The collected fractions were concentrated by ultrafiltration using Ultracel®10 kDa molecular weight cut-off (MWCO) membranes (Millipore, MA, USA) mounted on an Amicon®model 8200 stirred cell (model 8200; Millipore, CA, USA).

The concentrated sample (10 ml) was loaded onto a TSKgel2000SW column (Tosoh bioscience, Tokio, Japan), at a flow rate 0.7 ml/min, pre-equilibrated with 20 mM sodium phosphate buffer (pH 7.5) containing 150 mM NaCl. The column was calibrated with bovine serum albumin (66 kDa), carbonic anhydrase (29 kDa) and ribonuclease A (13.7 kDa). The yield of purified EstD11 was 9.3 mg/g of cell pellet (wet weight).

2.2.8. Electrophoresis and zymogram analysis

SDS–polyacrylamide gel electrophoresis (SDS–PAGE) was performed with a 15% separating gel on a vertical slab mini gel apparatus (Model SE 250; Amersham Biosciences) at 40 mA for 2 h. Gels were stained for protein detection with Coomassie Brilliant Blue R-250 following standard procedures. After electrophoresis, detec-

tion of hydrolytic activity was carried out following procedures described in Fuciños et al. [38], that essentially consisted on an in-gel renaturation process done by washing for 20 min at 50°C in 20 mM Tris–HCl buffer (pH 8.0) containing 0.5% (w/v) Triton X-100 followed by activity detection at 40°C using α-naphthyl acetate as substrate.

2.2.9. Synthesis of p-nitrophenyl (pNP) substrate library

The synthesis of *p*NP substrates was done by mild esterification of the corresponding carboxylic acid derivative with *p*-nitrophenyl chloroformate in presence of triethylamine and a catalytic amount of 4-dimethylaminopyridine [39] (See Table S1 for more detailed experimental procedures). The obtained product was purified by silica gel column chromatography (ethyl acetate-hexanes mixtures as eluant) affording the corresponding *p*NP ester derivative in medium to high yields (55 to 98%, Table S1) and high HPLC calculated purity (96% and higher).

2.2.10. Synthesis of (R,S) ibuprofen methyl- propyl- butyl esters and (R, S) naproxen methyl ester

Racemic acid (ibuprofen or naproxen, 1 eq.) was dissolved in the corresponding primary alcohol (methanol, *n*-propanol, *n*-butanol), mixed with H_2SO_4 (2 eq.) and refluxed under magnetic stirring overnight. The reaction was monitored by thin layer chromatography (TLC) analysis (3:7 ethyl acetate/*n*-hexane). Deionized water was added to the reaction mixture and then extracted twice with CH_2Cl_2. The organic layer was dried over anhydrous sodium sulphate, evaporated under reduced pressure and the residue was finally purified by column chromatography (3:7 ethyl acetate/n-hexane). The purity of the obtained esters (greater than 99%) was determined by HPLC-MS and 1H NMR analysis.

2.2.11. Other analytical methods

Cell density was monitored spectrophotometrically at 600 nm.

Protein was measured using the detergent-compatible BCA protein assay (Pierce, Rockford, IL, USA) using bovine serum albumin as standard

During cultivation, purification, biochemical characterization and unless otherwise stated EstD11 activity was determined with *p*-nitrophenyl decanoate (*p*NP decanoate) as substrate (0.2 mM final concentration) at pH 8.5 at 60°C. For 250 μl of reaction mixture, 200 μl buffer was mixed with 25 μl of 2 mM *p*NP decanoate and incubated at 60°C for 3 min. 25 μl of EstD11 (diluted appropriately) was added, and the reaction proceeded for 10 min at 60°C. Reactions were stopped by the addition of 75 μl of ice cold 1 M Na_2CO_3 and 25 μl of 0.4 M $CaCl_2$. Tubes were immersed in ice for 5 min and centrifuged for 5 min at 4 °C and 13,000 × g. From each tube 200 μl of clear supernatant was transferred into transparent 96-well plate and absorbance at 400 nm was measured using a FLUOstar Omega (BMG Labtech, Offenburg, Germany). At 400 nm the extinction coefficient (ε) was determined as 1,316.80 L $mmol^{-1}$ cm^{-1} (R^2 = 0.9993, n = 3). All measurements were performed in triplicate. One activity unit is defined as the amount of enzyme that catalyzes the formation of 1 μmol of *p*-nitrophenol per minute under standard assay conditions.

2.2.12. Biochemical characterization

The pH-dependent activity was determined at 60°C. Buffers used were 0.1 M acetate (pH 4.4–5), 0.1 M sodium phosphate buffer (pH 6–7.5), 0.1 M Tris-HCl buffer (pH 8.0–9.5), 0.1 M glycine/NaOH (pH 10–11). The pH of buffers was adjusted at 60°C.

The temperature-dependent activity was determined in the range 40–80°C in 0.1 M Tris-HCl (pH 8.5). The buffers were adjusted to pH 8.5 at each assayed temperature.

Thermal inactivation was performed at 70°C. 200 μl aliquots of EstD11 (0.1 mg/mL of protein concentration in 20 mM sodium phosphate buffer, pH 7.5, containing 0.15 M NaCl) in PCR tubes were sealed with Teflon and incubated at 70°C for designated times. Each withdrawn aliquot was quickly cooled down, centrifuged at 14,000 × g for 15 s. Clear supernatants were stored at –20°C until analysis of enzyme activity.

In all previous analysis, residual activity was determined with *p*NP decanoate at pH 8.5 and 60°C as indicated in section *2.2.11*.

Structural stability was assessed by differential scanning fluorimetry (DSF) essentially as described in Niesen et al. [40]. The assay was done in 96-well PCR plates using a reaction volume of 100 μl. EstD11 in 20 mM sodium phosphate (pH 7.5), 150 mM NaCl at 0.1 mg/ml final concentration was mixed with the compounds screened and incubated 10 min at room temperature before adding SyPro Orange (Invitrogen, CA, USA). The EstD11 final concentration in the assays was 50 mM. Detergents and organic solvents were screened at 1%, and 10% (v/v) final concentration, respectively. LDAO (0–1.0 mM) in 20 mM sodium phosphate (pH 7.5) buffer containing 150 mM NaCl was added instead of test compounds in the control samples. All assays were done in triplicate. The plates were sealed with optical cap strips (Stratagene, CA, USA) and gradually heated in a qPCR machine Stratagene Mx3000P (Agilent Technologies, CA, USA) from 25°C to 95°C at 1°C/min. The fluorescence at 610 nm (excitation at 492 nm) was collected at every 1°C. Interference caused by LDAO (0–1.0 mM) was subtracted and data were processed with program GraphPad Prism 8.4.1 for Mac OS X (GraphPad Software, San Diego, CA, USA). To determine the melting temperature (Tm), a Bolzmann sigmoidal equation was fitted to the raw data [40].

2.2.13. Substrate specificity

2.2.13.1. Selectivity towards p-nitrophenyl (pNP) substrates. The substrate specificity was studied using 20 newly synthesized *p*-nitrophenyl esters (see Scheme 1 and Table S1). In addition, commercial *p*-nitrophenyl esters were also tested: butyrate (**16**), octanoate (**17**) decanoate (**18**), dodecanoate (**19**), tetradecanoate (**20**) and hexadecanoate (**21**).

All *p*NP esters were prepared in DMSO at 2 mM final concentration. To minimize autohydrolysis, activity was measured at 45°C in 0.1 M Tris-HCl (pH 8.5) , 0.1% (w/v) gum arabic and 1% (w/v) CHAPS, the two last added to increase the esters' water solubility. It was verified that CHAPS increased approximately 2.5-times hydrolytic activity of the *p*NP esters cyclohexanecarboxylate (**12**), butyrate (**16**), 3-methylbutanoate (**25**) and 2-methylheptanoate (**26**), but had no influence on substrate specificity (not shown). Reaction mixture consisted of 80 μl of reaction buffer (preheated to 45°C) and 10 μl of 2 mM *p*NP esters (0.2 mM in the assay) and was incubated at 45°C/3 min before adding 10 μl of EstD11 (0.15 μg/ml in the assay). Reaction was followed at 400 nm for 20 min (every 20 s) in a microplate reader FLUOstar Omega (BMG Labtech, Offenburg, Germany). Assays were done in triplicate and values were corrected for nonenzymatic hydrolysis. Only linear portions of progress curves were considered for determining lipolytic activity. Media values and SDs were calculated using the GraphPadPrism v.8.4.1 for MacOSX software. The substrate with the highest activity was set to 100% and the percentage of relative activity for the remaining adjusted accordingly.

2.2.13.2. Selectivity towards fluorescein derivatives. The fluorogenic substrates fluorescein dihexanoate (FdC6), fluorescein dioctanoate (FdC8) and fluorescein dilaurate (FdC12) were used for measuring EstD11 activity on esters with bulky aromatic alcohol moieties and aliphatic chains of different length on the acidic side. Fluorescein substrates were dissolved in cellosolve to obtain 10 mM solutions (stock 1). From this a new dilution in cellosolve was done to obtain new stocks in the concentrations range 0.1 and 50 μM. The 100 μl reaction mixtures were prepared directly on 96-well plates for

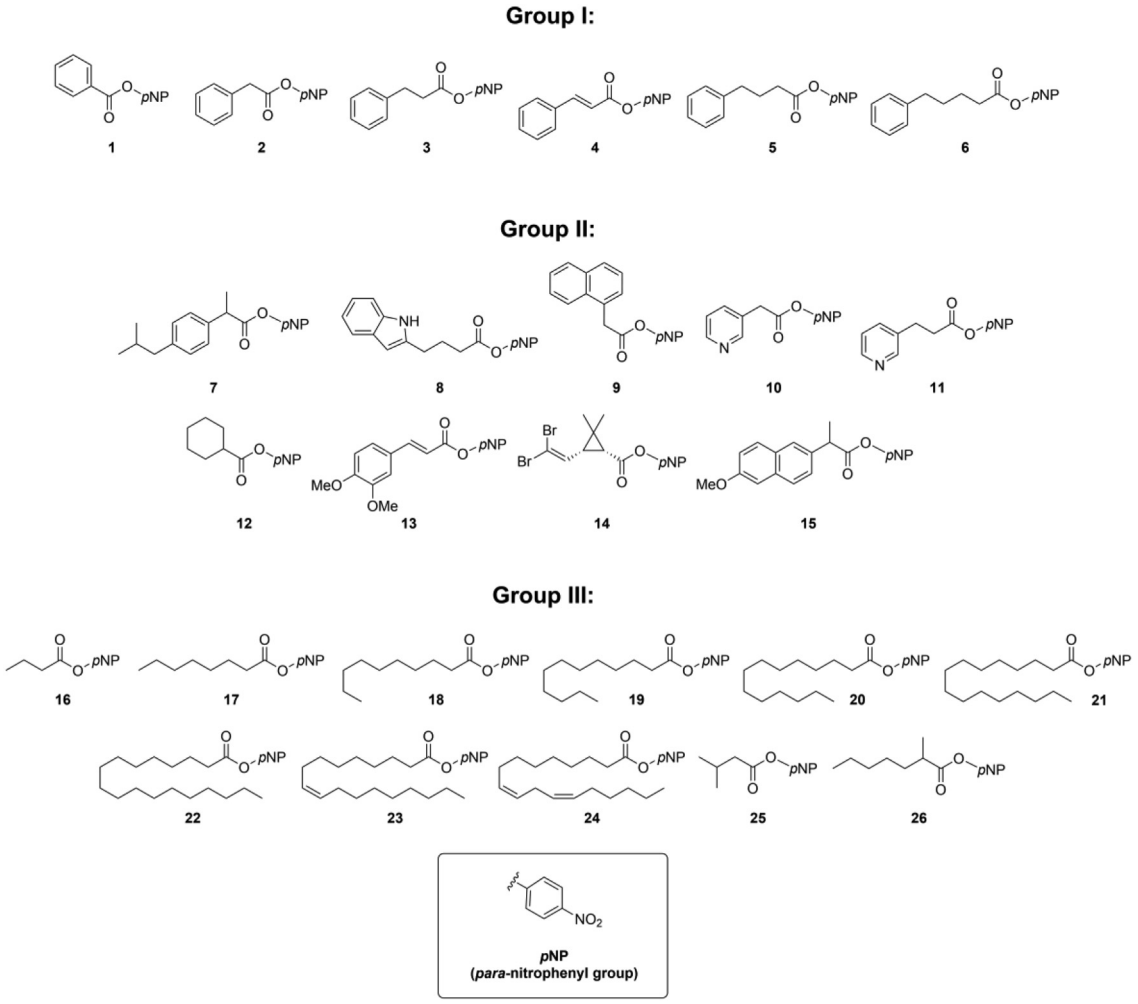

Scheme 1. Library of chromogenic esterase substrates. Each substrate is composed of *p*NP and diverse groups organized into three categories: Group I encloses esters with phenyl groups on the carboxylic side, Group II with aromatic and cycloalkyl esters and Group III with aliphatic carbon chain of different length and saturation. All were synthesized as described in section 2.2.9.

qPCR by mixing 80 μl reaction buffer (20 mM Tris-HCl pH 8.5/60°C), 10 μl fluorescein from the second stocks, 10 μl EstD11 (diluted as described below) and tightly sealed with transparent foil. Change in the fluorescence due to the release of fluorescein (SYBR Green filter: λ_{ex} = 492 nm; λ_{em} = 516 nm) was measured at 60°C for 10 min using a qPCR machine Stratagene Mx3000P (Agilent Technologies). All measurements were performed in triplicate and were corrected for nonenzymatic hydrolysis (background rate). A fluorescein calibration curve in the range 0.01 and 0.25 μM was done using the same buffer as for the enzymatic assay (slope = 199,027.75; intercept = 4,743.98; R^2 = 0.9954). The experimental data were fitted to Michaelis-Menten models with and without substrate inhibition at 95% confidence using GraphPad Prism 8.4.1 software. Details about the calculation of initial reaction rates are described in the Results and Discussion section.

EstD11 was conserved in concentrated stock solutions (4.4 mg/ml) in buffer. These solutions were 100-fold diluted in water with 0.5% (w/v) CHAPS and kept for 15 min at room temperature. The final working enzyme solution (0.15 μg/ml) was obtained after a second 100-fold dilution in 20 mM Tris buffer pH 8.5 (at 60°C) and 150 mM NaCl with 10% cellosolve, and 15 min of resting at room temperature.

2.2.13.3. Enzymatic hydrolysis of ibuprofen and naproxen esters. Racemic esters (0.136 mmol) were dissolved in the organic cosolvent (10% v/v) and added to EstD11 (0.5 U, measured with *p*NP decanoate as indicated in 2.2.11) dissolved in 0.1 M Tris-HCl buffer (pH 8.5). The reaction mixture was agitated under magnetic stirring at 60°C or 80°C. Reactions were then diluted with methanol, filtered and analyzed by HPLC-MS.

The content of ibuprofen, ibuprofen esters, naproxen, naproxen methyl ester were analyzed by HPLC-MS. Column = Luna C18; Eluent = mobile phase A (1:1 acetonitrile/MeOH), mobile phase B (water), mobile phase C (100 mM ammonium acetate pH 7); flow rate = 0.30 ml/min; column temperature = 35°C. Initial chromatographic conditions were 10% A, 85% B, 5% C with 3 min hold followed by a gradient to 95% A, 0% B, 5% C with 9 min hold.

The optical purity of ibuprofen and naproxen was determined by HPLC using chiral column ChiraCel OD-H 5 um separating the *S*- and *R*-enantiomers and comparing with the standard resolved ibuprofen enantiomer. Column temperature = 25°C; mobile phase = 1:100:0.1 isopropanol/n-hexane/TFA; flow rate = 1 ml/min; peaks detection: 220 nm.

Enantioselectivity of EstD11 for the hydrolysis of ibuprofen and naproxen esters was evaluated and expressed as the enantiomeric excess (*ee* value) and the enantiomeric ratio (*E*-value) of the products of the reaction. Conversion was calculated as the percentage of ester hydrolyzed; *ee* value was calculated as the difference between the molar fraction of the *R* and *S* enantiomers and expressed as percentage; *E*-value was calculated as follows when

the percentage of substrate conversion was equal or greater than 30%:

$$E = \frac{\ln[1 - c \times (1 + ee)]}{\ln[1 - c \times (1 - ee)]} \quad (1)$$

2.2.14. Structural studies

2.2.14.1. EstD11 crystallization. Protein crystallization was pursued thought high-throughput techniques using several Hampton commercial crystallization screens with the *Innovadine* Crystallization Robot. Conditions producing crystals were optimized by sitting-drop vapor-diffusion method at 18°C mixing 1 μl of the protein solution and 1 μl of precipitant, equilibrated against 150 μl of precipitant solution in the reservoir. The condition that succeeded in getting best quality crystals contains sodium formate 3.2 M and citrate 0.1 M, pH 5.

Crystals were typically observed after 1 week at 18°C. Crystals grown were cryo-protected by using a 50:50 paratone/paraffin mixture before flash-frozen in liquid nitrogen.

2.2.14.2. Soaking and co-crystallization experiments. For both soaking and co-crystallization trials, all ligands: *p*NP 2-(6-methoxynaphthalen 2-yl) propanoate (Naproxen *p*NP ester, **15**), methyl-naproxen (**30**), *p*NP-cyclohexanecarboxylate (**12**) and fluorescein, were dissolved in acetone at a stock concentration of 150 mM and a final concentration of 25 mM.

In the case of EstD11:naproxen complex 1 and 2, EstD11-S144A:methyl-naproxen, EstD11 S144A:naproxen-pNP complex and EstD11:*p*-nitrophenol structures, structures were obtained by the co-crystallization method. For EstD11:NP complex 1 and EstD11 S144A:naproxen-pNP complex, the Naproxen *p*NP ester substrate was incubated with the protein sample, at a final concentration of 10 mg/ml protein and 3 mM of ligand, for 30 min at 30°C prior to crystallization. Then, the mixture was subjected to the crystallization conditions described above.

EstD11:naproxen complex 2, EstD11-S144A:methyl-naproxen complex and EstD11:*p*NP complex were obtained at room temperature (18°C) by mixing 1 μl of the protein and 0.2 μl of the ligand, with a final concentration of 25 mM of methyl-naproxen and *p*NP-cyclohexanecarboxylate respectively, with 1 μl of the reservoir during the crystallization experiment, without a preincubation stage.

Structures for EstD11:cyclohexane-carboxylate and EstD11:fluorescein complexes were obtained by soaking the native protein crystals with 1–5 mM of the ligand at 30°C 30 min and then, maintained at 18°C up to a maximum of 2 months.

2.2.14.3. Data collection, phasing and model refinement. Diffraction data was collected in the XALOC beamlines at the ALBA synchrotron, using the Pilatus 6 M detector. Crystals diffracted up to 1.20–2.28 Å resolution and belonged to the P $2_12_12_1$ space group, except for the cases of EstD11:naproxen complex 1 and EstD11 S144A:naproxen-*p*NP complex, belonging to the I 222 space group. Crystallographic data collection and refinement statistic are summarized in Table S3.

The collected datasets were processed with XDS [41] and Aimless [42]. In all the P $2_12_12_1$ crystals, two monomers were encountered in the asymmetric unit, with a 41–42%. of solvent content. In contrast to the above, in I 222 crystals only one monomer was found in the asymmetric unit, yielding a Matthews coefficient of 2.03–2.07 $Å^3$/Da and a solvent content of 39.5–40.6%.

Structure determination was performed by the molecular replacement method using the E40 HSL esterase from *E. coli* (PDB code 4XVC) which shares a 57% identity with EstD11. Finally, the model was manually completed using Coot [43] followed by refinement using PHENIX [43] and REFMAC5 [44]. A summary of the refinement statistics is given in Table S3.

3. Results

3.1. Construction of metagenomic library and identification of the lipolytic gene EstD11

A fosmid library (RCWL2) consisting of approximately 132,000 clones with an average insert size of 35 Kb (ranging from 24.5 Kb to 50.1 Kb) was constructed from metagenomic DNA isolated from the Río Caldo (Lobios, Spain) hot spring water. The library was arrayed into 96-well plates, at a density of 2,000 clones per well, and screened for lipolytic activity and one halo of clearance appeared around the well D11 in tributyrin agar plates after incubation at 37°C (Fig. S1). The positive fosmid clone (pCT3FK-EstD11) was isolated, sequenced and an ORF encoding for a putative lipase/esterase gene (named EstD11) was identified. The sequence was submitted to GenBank with the accession number BankIt2412597. The EstD11 ORF encodes a predicted protein of 296 amino acid residues, with a calculated molecular mass of 32,153.05 Da and a pI of 5.21.

BLASTp search of the NCBI database indicated that identified esterase EstD11 showed 68% sequence identity to the organic solvent-tolerant esterase EstC23 derived from the soil metagenome [45]. Based on sequence analysis, the EstD11 belong to lipase family IV (Fig. 1), which is the HSL family [12].

3.2. Protein expression and purification

The EstD11 enzyme was successfully cloned and overexpressed in *Escherichia coli* and purified using a thermal precipitation step followed by hydrophobic and SEC chromatography. The enzyme was purified 12-fold with a final specific activity of 21.7 U/mg (Table S1). The molecular weight of EstD11 was 32.1 kDa according to the profiles in SEC, SDS-PAGE and zymogram analysis (Fig. S2), that matched that deduced from the primary sequence indicating that EstD11 was a monomer in solution.

3.3. Biochemical characterization

3.3.1. Effect of pH and temperature on the enzyme activity and stability

EstD11 was assayed for activity in buffer at various pH values. Due to instability issues at elevated temperatures of *p*NP esters with short acyl chains, *p*NP decanoate was used as a substrate. pH values higher than 9.0 promoted excessive substrate self-hydrolysis and therefore they were not tested. EstD11 showed no activity at acidic pH, but rapidly increased around neutral pH. It displayed maximal activity in a wide pH range (6.5–8.0) and decreases to 84% at pH 8.5 and 57% at pH 9.0 (Fig. 2A).

The optimal reaction temperature for EstD11 was 60°C which is 17°C lower than the temperature of the source environment (77°C) and displays approximately 40% of residual activity at 70°C (Fig. 2B). After 1 h incubation at 70°C the enzyme recovered partially the activity reaching 70% of that measured at 60°C, but it was almost entirely lost after 3 h of incubation (data not shown). EstD11 showed only 30% activity at 50°C and<10% of maximal activity when incubated at 40°C.

3.3.2. Effect of organic solvents on enzyme activity

EstD11 hydrolytic activity was studied in the presence of 10% (v/v) of several organic solvents (methanol, ethanol, isopropanol and *n*-butanol, acetonitrile and DMSO). Activity was measured with *p*NP decanoate and compared with buffer without additives.

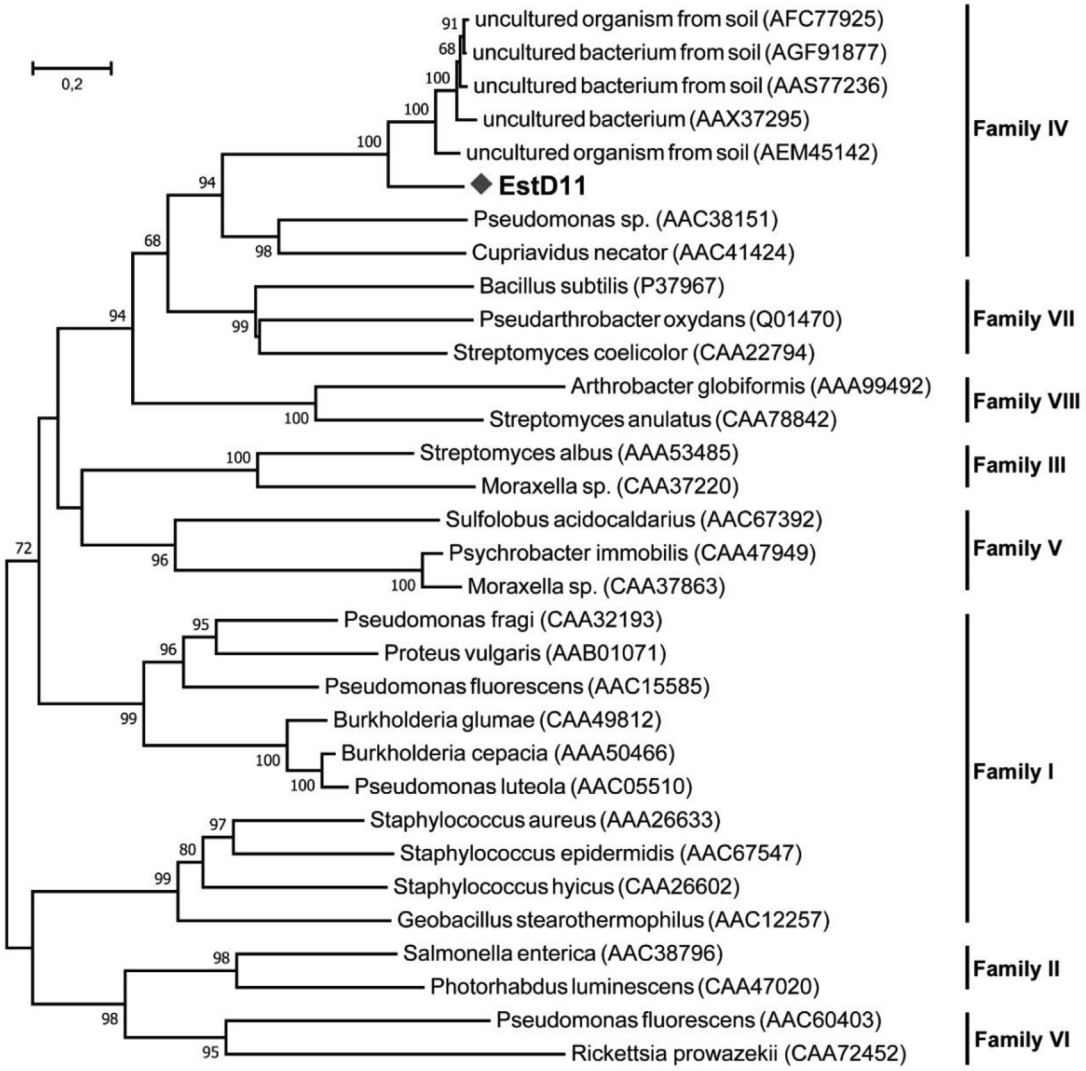

Fig. 1. Neighbor-joining phylogenetic tree based on amino acid sequence of the EstD11. It shows top 5 sequence homologues of EstD11 and known members of lipase families I-VIII. Esterase identified in this study is shown on bold. GenBank accession numbers of the reference sequences are shown in parentheses. The tree was drawn using MEGA7 software, with Poisson correction method and 1000 bootstrap replications. Only bootstrap values higher than 50% are shown.

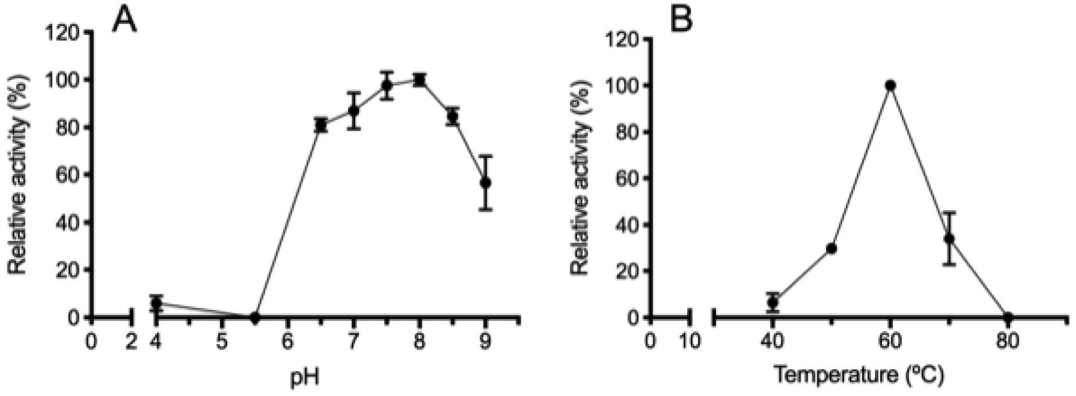

Fig. 2. Effect of pH (A) and temperature (B) on EstD11 activity. The enzyme activity was measured with 0.20 mM *p*NP decanoate as a substrate at 60°C. (**A**) Relative EstD11 activity at different pHs: pH 4.0 and 5.5 (80 mM sodium acetate), pH 6.0 – 7.5 (sodium phosphate) and pH 8.0 – 9.0 (Tris-HCl). pH for all buffers was adjusted at 60°C. Maximal activity reacahed in Tris-HCl at pH 8.0 was considered as 100% (0.847 U/mg). (**B**) Relative EstD11 activity at different temperatures. EstD11 activity was tested in reaction buffer (80 mM Tris-HCl pH 8.5). pH was adjusted for each temperature separately. Activity value obtained at 60°C was taken as 100% (0.540 U/mg). Data are given as means ± SD, n = 3. EstD11 concentration in the assay was 0.044 μg/ml.

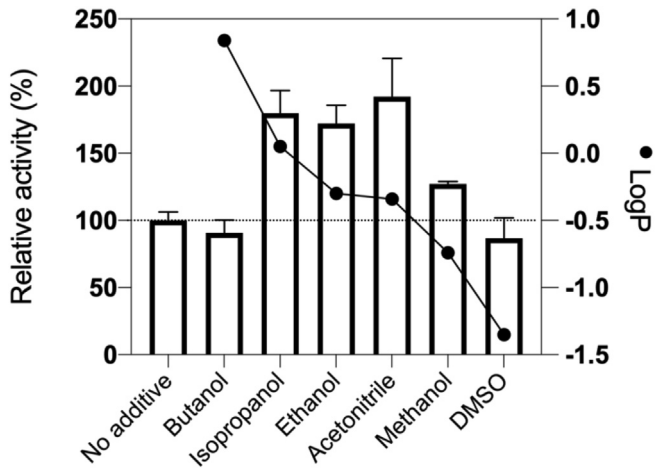

Fig. 3. Effect of organic solvents on EstD11 activity. Final concentrations were 10% (v/v) of each organic solvent. Enzyme activity was measured with *p*NP decanoate at 60°C. 100% activity was 0.787 ± 0.051 U/mg (3 min incubation). EstD11 concentration in the assay was 0.044 μg/ml. Data are given as means ± SD, n = 3. LogP values inserted in the figure (•) were from [46,70].

Important increases in EstD11 activity were observed with isopropanol, ethanol and acetonitrile (almost twice more active) whereas DMSO and *n*-butanol inhibited only slightly EstD11 activity (Fig. 3). The log P parameter (defined as logarithm of the partition coefficient of the solvent between *n*-octanol and water) was used as an index of the solvent polarity (Fig. 3). Organic solvents with low Log P (more hydrophilic) are known to be more toxic for many enzymes due to stripping essential water molecules off the enzyme structure [46], or interactions with the active site modifying the essential network of hydrogen bonds for catalysis [47]. Nonetheless none of the assayed solvents inhibit noticeably EstD11 activity and, on the contrary, some of them activate it. It has been reported that alcohols may increase enzyme's activity by increasing substrate's solubility in the immediate vicinity of the catalyst [46]. Apart from *n*-butanol, this activating effect dominates for isopropanol, ethanol and, in a lesser extent, methanol. Additionally, alcohols with higher hydrophobicity (high LogP) may hinder the access of water molecules to the active enzyme center. This might be the case of *n*-butanol with the highest LogP (0.84) of the assayed alcohols and also with a chain length that, as discussed below, coincides with that of the best EstD11 substrate (*p*NP butyrate) and, at the employed concentration, might act as a competitive inhibitor [48].

3.3.3. Structural stability. Differential scanning fluorimetry (DSF) analysis

The structural stability of EstD11 esterase against thermal denaturation mediated by several chemical additives was measured by DSF. Recordings of fluorescence intensity versus temperature for EstD11 dissolved in buffer started with a high fluorescence intensity and lacked a clear transition curve precluding the calculation of a value for the T_m (Fig. 4A). The presence of interfering hydrophobic compounds such as detergents, protein aggregates or solvent-exposed hydrophobic patches can cause high fluorescence background at low temperatures [49]. As the EstD11 sample used for DSF experiments was recovered as a single peak by gel filtration chromatography at the expected MW and no additives were included in the sample, we favor for the presence of solvent-accessible hydrophobic areas in EstD11 native folded state where the binding of the dye occurs already at low temperature. Incorporation of detergents to protein samples normally increases fluorescence possibly due to dye binding to detergent micelles [50]. Balancing the ratio of protein to detergent concentration in the sample enabled Pantoliano and coworkers to conduct DSF experiments on the membrane protein bacteriorhodopsin using *n*-nonyl-β-D-glucopyranoside at 6.4 mM concentration (approx. CMC_{H2O}) [51].

By applying this approach, we investigated the effect of the zwitterionic surfactant LDAO at two concentrations: 0.5xCMC and 1.5xCMC (CMC_{H2O} = 1 mM). Fig. 4B shows that at 0.5xCMC, initial fluorescence still kept high although the transition curve was better defined than in the absence of LDAO. Above the CMC (Fig. 4C), an increase in the steepness of the melting transition was displayed mainly due to the decrease in the fluorescence at low temperatures. The EstD11 melting temperature was dependent on LDAO concentration; below CMC it was 76.49 ± 0.18 (R^2 = 0.9440) but decreased to 67.41 ± 0.22 (R^2 = 0.9478) when LDAO was forming micelles. This temperature was more than 10°C higher than the optimal temperature for activity of the enzyme (see above). As will be shown below, the failure to obtain a denaturation curve for EstD11 in absence of LDAO did not impair its crystallization as it has been observed for other proteins [49].

The influence of detergents (1% v/v) and organic solvents (10% v/v) on EstD11 T_m was examined, including 1.5 mM LDAO in all samples. Triton X-100, Tween-80, SDS completely destabilize protein structure (not shown), whereas CHAPS, a zwitterionic detergent as LDAO, shifted its melting point from 67.41 ± 0.22 (without CHAPS) to 76.90 ± 0.185°C (with CHAPS; R^2 = 0.9682) (Fig. 4D). Literature on the negative effect of SDS, Triton X-100 or Tween 20 is abundant [52–54] as well as on the positive effect of CHAPS on activity and stability of a number of esterases [53].

Concerning the organic solvents, their incorporation into the sample, even though the presence of LDAO, gave rise to a high fluorescence background at low temperatures. SYPRO Orange has low quantum yield in aqueous solution but is highly fluorescent in nonpolar environments with low dielectric constants [55] as likely is provided by the organic solvents assayed, with dielectric constants in the interval 17.51 to 46.45 [46]. As a result, melting curves were very flat-shaped, and the fluorescence signal too low to allow an accurate T_m calculation for most of the assayed solvents. For DMSO, T_m resulted 73.77 ± 0.25 °C (R^2 = 0.8786), which is more that 6°C higher than that determined for EstD11 in the presence of micellar LDAO (67.41 ± 0.22) (Fig. 4E). The reported ability of DMSO media in reducing protein aggregates and increase enzyme solubility by avoiding hydrophobic interactions amongst hot regions on the lipase structure, might explain the gain in structural stability of EstD11 with DMSO in the thermal shift experiments [56].

3.4. Kinetic characterization

3.4.1. Substrate specificity on p-nitrophenyl carboxylic esters

A library of 20 newly synthesized *p*NP derivatives and 6 commercially available aliphatic *p*NP esters was used to analyze the substrate specificity of EstD11. According to the acidic moiety of the ester bond, substrates fall into three groups: Group I composed by phenyl esters with different linker length and saturation, Group II made by aromatic and cycloalkyl esters, and Group III aliphatic carbon chain of different length and saturation (Scheme 1 and Table S1).

The library includes several carboxylic moieties of industrially interest (food, pharmaceutical, and bioremediation industry), such us naproxen (**15**), ibuprofen (**7**), ferulic acid (**13**) or deltamethrin (**14**) in order to reveal the potential use of new identified lipolytic enzymes for industrial applications or detoxification of pyrethroid pesticides, as well as esters with interest to deepen on the enzyme active site architecture. Hydrolysis was followed at 45°C (T_{op} for EstD11 was 60°C) to lower the rate of autohydrolysis. Despite that, immediate autohydrolysis of the *p*NP esters 2-phenylacetate (**2**), 2-

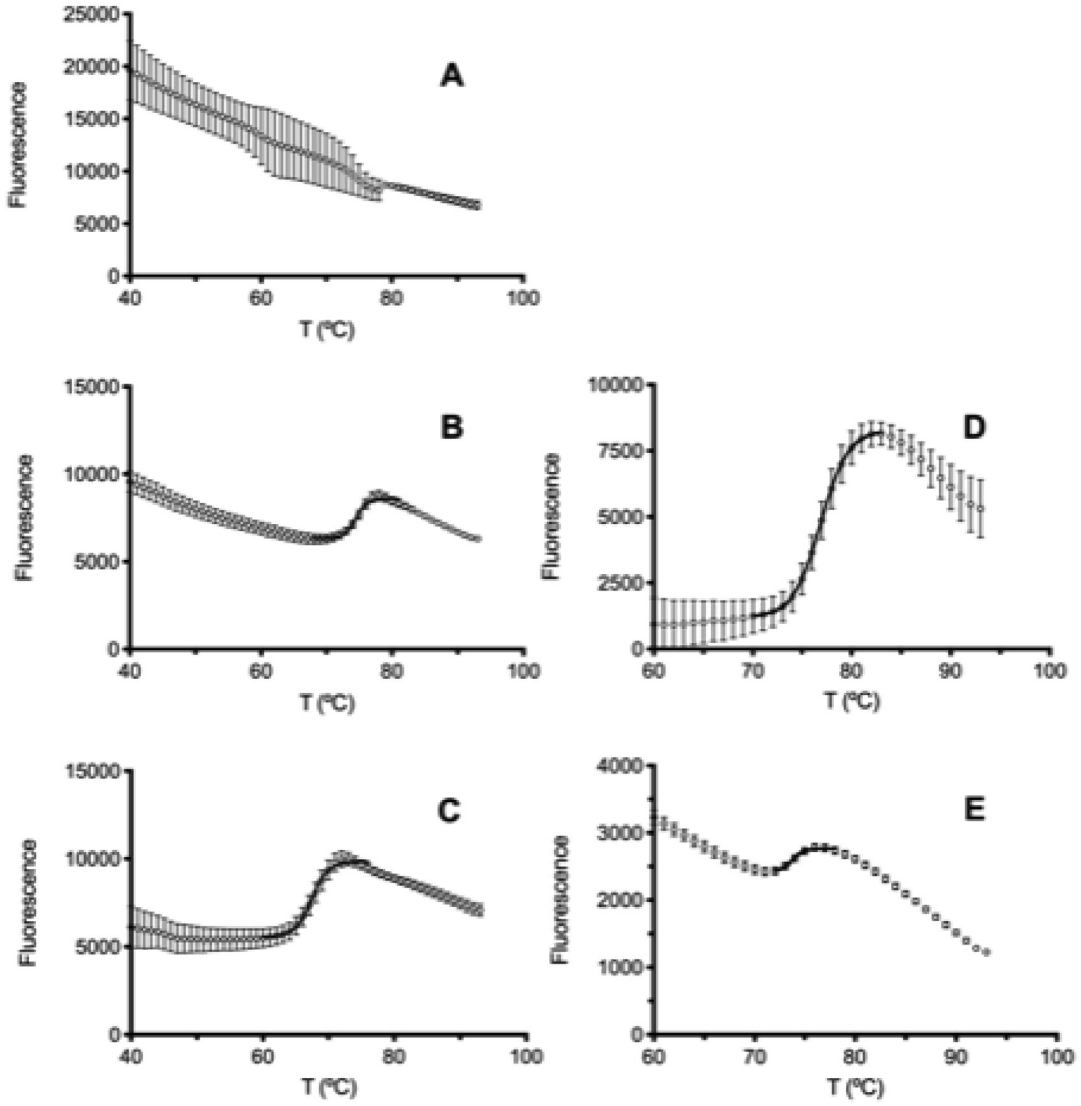

Fig. 4. EstD11 structural stability by DSF analysis. Melting curves of EstD11 (0.1 mg/ml) in (**A**) reference buffer, 20 mM sodium phosphate containing 150 mM NaCl, (pH 7.5) (**B**) reference buffer supplemented with 0.5 mM LDAO (0.5xCMC) and (**C**) with 1.5 mM LDAO (1.5xCMC) (**D**) 20 mM sodium phosphate buffer (pH 7.5) containing 150 mM NaCl and 1.5 mM LDAO supplemented with 1% (w/v) CHAPS and (**E**) the same buffer as in D but supplemented with 10% (w/v) DMSO. Data are given as means ± SD, n = 3. The black line represents the non-linear fit of the fluorescence curve to the Boltzmann equation.

(naphthalen-1-yl)acetate (**9**), 2-(pyridin-3-yl)acetate (**10**) and 3-(pyridin-3-yl)propanoate (**11**) was observed, therefore they were excluded from the screening.

The far best substrate for EstD11 was the cyclohexyl ester, *p*NP cyclohexanecarboxylate (**12**) (Fig. 5). Interestingly, activity on *p*NP benzoate (**1**) was nearly zero pinpointing the constrain imposed by the aromaticity in the cyclohexyl ring attached to the ester bond to the catalysis. Extending the linker between the ester and the phenyl ring by adding two (*p*NP 3-phenyl propanoate, **3**), three (*p*NP 3-phenyl butanoate, **5**) or four (*p*NP 3-phenyl pentanoate, **6**) methylene groups, enzyme activity increased an average of 20-fold, without big differences amongst them. However, if an α/β-double bond was introduced in the aliphatic space (*p*NP 3-phenyl cinnamate), activity was completely abolished (**4** *vs* **3**).

Therefore, phenyl groups on the carboxyl moiety of the ester are not accepted by EstD11unless the ring is moved apart from the scissile ester bond and the linker does not contain an α/β-unsaturation. The unsaturated linker might also account for the scarce activity of EstD11on the ferulic acid derivative of *p*NP (**13**).

In contrast to other bacterial hydrolases that show minimal activity toward cycloalkyl substrates (aromatic and nonaromatic) [57,58], FTT0941c esterase from *Francisella tularensis* behaves as EstD11 on substrates with cyclohexyl rings appended to esters bonds but, unlike EstD11, FTT0941c activity on the substrate with aromatic ring and the nonaromatic is similar [59]. As for EstD11, the relative attachment distance from the ester bond to the phenyl group greatly influenced the relative catalytic activity of FTT0941c, but in the opposite direction (insertion of just a methylene group decreases activity of FTT0941c by a factor of 10 but increases 20 times for EstD11) [59].

Group III of *p*NP esters, contains the second-best substrate for EstD11, *p*NP butyrate (**16**), with 50% the activity measured with **12,** but activity declines progressively as the length of the aliphatic chain increases (**17**–**22**). No activity was detected for *p*NP with long unsaturated acyl chains (**23**, **24**).

Short aliphatic chains are not the only requirement for EstD11, as if branches are introduced in α or β positions relative to the carbonyl group, activity decreases noticeably as seen for substrates **26** (*p*NP 2-methylheptanoate) and **25** (*p*NP 3-methylbutanoate),

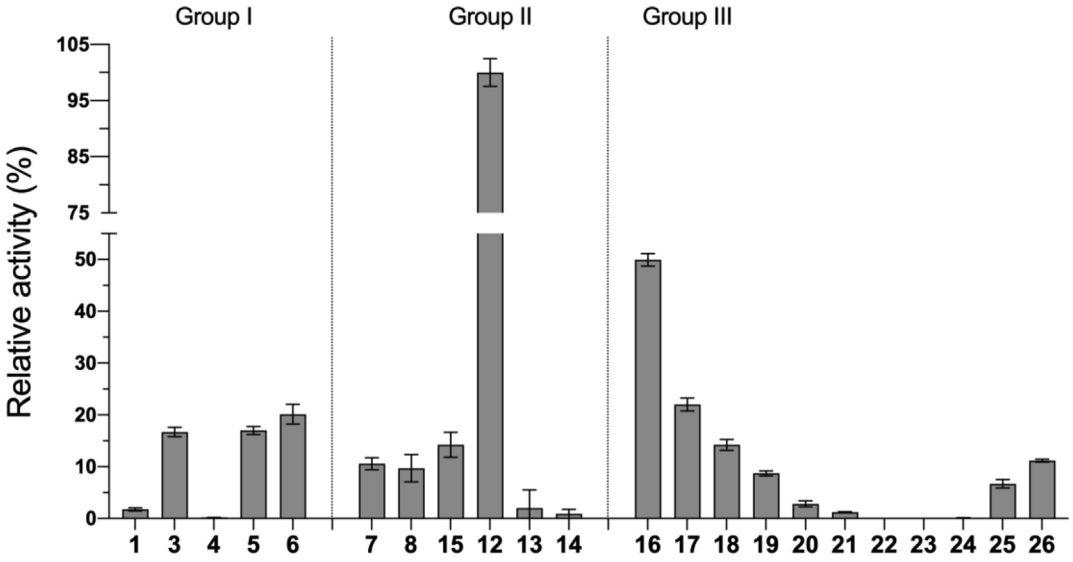

Fig. 5. Specific activity of EstD11 against a set of structurally diverse esters. Substrate profile of EstD11 enzyme against the *p*NP esters. Activity was measured at 45°C in 0.1 M Tris-HCl pH 8.5 buffer, containing 0.1% (w/v) gum arabic and 1% (w/v) CHAPS. Substrate concentration in the assay was 0.2 mM and enzyme 0.15 μg/mL. 100% activity was 2.51 ± 0.12 U/mg protein. Data are given as means ± SD, n = 3.

respectively, for which activity was, respectively, 30% and 50% the activity measured with the closest *p*NP ester in terms of chain length (*p*NP octanoate, **17**). This negative effect of ramification might also contribute to the low activity on ibuprofen (**7**) and naproxen (**15**) esters as they possess branched linkers next to the scissile ester bond and were hydrolyzed by EstD11 with 11% and 14% the activity of the best substrate **12**, respectively.

3.4.2. Substrate specificity on fluorescein di-carboxylic esters

To get more insight about the preference of EstD11 for medium chain fatty acids, fluorescein derivatives of C6 (FdC6), C8 (FdC8) and C12 (FdC12) were assayed. These substrates offer the advantage of being more stable towards autohydrolysis than *p*-nitrophenyl derivatives, thus allowing working at optimal conditions for EstD11 (pH 8.5 and 60°C) without significant autohydrolysis for all the substrate concentrations tested (between 0.1 and 50 μM). Additionally, these fluorescein derivatives harbor a bulky alcohol moiety that may give additional insights on structural features of EstD11 for the alcohol moiety of aliphatic esters. When working with these substrates, it must be considered that their kinetics of hydrolysis often show sigmoidal profiles, as happened for most of the conditions here assayed (Fig. S3). This is due to the presence in the same molecule of two scissile ester bonds, which can be hydrolyzed by the enzyme in a generally recognized two-step mechanism [60]. As a consequence, the mono-substituted derivative is generated as a low fluorescent intermediate product, which is also a new substrate for the enzyme. Therefore, at any reaction time the detected fluorescence is the sum of the fluorescence of both products (the mono-substituted fluorescein and free fluorescein), each of them contributing depending on their specific fluorescence and relative concentrations, which are also dependent on the respective reaction rates of formation.

Under these circumstances a way to proceed is to consider the very first moments of reaction when the mono-substituted fluorescein is the major product of reaction and the main contributor to fluorescence. Therefore, in this work the initial reaction rates were calculated as the slope of the curve during the first 2 min of reaction, which showed good linear fits (R^2 between 0.96 and 0.99), and keeping the percentages of hydrolyzed substrate below 7% applying the same criterium used by Zisis et al. [61] for the hydrolysis of fluorescein di-acetate. The reaction rates thus calculated were multiplied by 30 to match the fluorescence of the mono-substituted fluorescein to that of free fluorescein applying the estimated conversion factor used for different moieties such as acetate [61] or β-galactopyranoside [62] and finally transformed into enzyme units using a calibration curve made with fluorescein. These initial rates were fitted to Michaelis-Menten (MM) and Substrate Inhibition Models for the estimation of the kinetic parameters (V_{max}, K_M, k_{cat} and k_{cat}/K_M).

The results shown in Table 1 (see Fig. S4 for kinetics) confirm the preference of EstD11 for short chain fatty acids, as with the *p*-nitrophenol derivatives. While V_{max} was similar for the three fluorescein dicarboxylic derivatives, K_M clearly increased with the number of carbons of the acyl chain, being the increment more drastic between 6 and 8 carbon atoms than between 8 and 12, as also the specificity constants shows. It is noteworthy to say that while for the FdC8 and FdC12 substrates only the MM model fitted properly, in the case of FdC6 the experimental data were better described by the MM with substrate inhibition. Although we have no data to support it, a possible hypothesis for explaining it could be the more advanced state of the reaction with the shorter substrate, that could generate a higher transient accumulation of the mono-substituted derivative with low reaction rates due to a hypothetical higher K_M than the di-substituted substrate, as Fielder et al. [60] calculated for the mono-substituted fluorescein β-D-galactoside when studying the hydrolysis of fluorescein di-β-D-galactoside by β-galactosidase.

3.4.3. Enantiomeric hydrolysis of racemic ibuprofen and naproxen esters

Enzymatic kinetic resolution has become a useful method to produce pure compounds requiring very high enzyme enantioselectivity. Ibuprofen and naproxen are both non-steroidal drugs (NSAIDs) showing general structural features, a 2-aryl substituted propionic acid containing a stereogenic center. It is well known that for both molecules the active form is the *S*-enantiomer. In order to understand the biocatalytic properties of EstD11, the enzyme was used to hydrolyze ibuprofen and naproxen esters under varied conditions.

3.4.3.1. Ibuprofen esters hydrolysis. Some preliminary trials were performed to identify starting reactions conditions. Absence of

Table 1
Michaelis-Menten (MM) kinetic parameters of EstD11 with different chain length fatty acid fluorescein derivatives.[1]

Substrate	Model	V_{max} (U/mg)	K_M(μmol)	K_i(μmol)	r^2	$K_{cat}(s^{-1})$	$k_{cat}/K_M(s^{-1}\ mM^{-1})$
FdC6	MM	1.42	0.10	–	0.9300	0.8	7,961.6
FdC6	MM with Substrate Inhibition	1.66	0.13	15.94	0.9522	0.9	6,667.7
FdC8	MM	1.35	1.41	–	0.9764	0.7	510.6
FdC12	MM	1.79	4.37	–	0.9970	1.0	218.4

[1] Activity was measured following the change in the fluorescence due to the release of fluorescein (SYBR Green filter: λ_{ex} = 492 nm; λ_{em} = 516 nm) at pH 8.5 and 60°C for 10 min using a qPCR machine Stratagene Mx3000P (Agilent Technologies).

the ionic detergent CHAPS and a temperature of 60°C were set as default conditions (scheme 2) then a co-solvent screening (10% v/v) was performed.

In absence of co-solvents EstD11 hydrolyzed ibuprofen methyl ester (**27**) with a good conversion of 50.15% but low enantioselectivity with 30.44% as *ee* value. A number of co-solvents were assayed (ethanol, methanol, propanol, butanol, DMF and DMSO) with different conversion outcomes; maximum of 68.01% (*ee* value 36.02%) with DMSO and only 1.04% with *n*-butanol.

Considering the thermophilic character of EstD11, hydrolysis of ibuprofen methyl ester (**27**) to the *R*-corresponding acid was assayed at 80°C and 10% DMSO to test the effect of temperature on the enantioselectivity of the reaction in these extreme conditions. As expected, the enzyme was able to preserve some activity and convert 17.95% of the substrate. Different percentages of DMSO were tried but either the enzyme activity was completely inhibited or was very low (data not shown). Chiral data performed for 10% DMSO showed that *ee* values improve in favor of the *R*-enantiomer (*ee* 75.54% compared with 30.44% at 60°C). Apart from methyl, propyl and butyl esters of ibuprofen were also tested with EstD11 at 80°C (Table 2). Conversion achieved in the hydrolysis of ibuprofen propyl and butyl esters did not improved that obtained for the methyl ester, but for the reaction with butyl ester (**29**) it was possible to perform chiral analysis giving an *ee* of 89.94% for the *R*-enantiomer. Taking these results together with those previously presented, a chain length of 4C atoms gives rise to good substrates for EstD11 no matter it is located on the alcohol (ibuprofen esters) or the acid moiety (*p*NP and fluorescein) of the esters.

3.4.3.2. Naproxen esters hydrolysis. Reaction conditions used for the resolution of the racemic naproxen methyl ester (**30**) were selected considering results obtained with ibuprofen methyl ester (**27**). Specifically, DMSO 10%, MeOH 10%, 0.5 U of EstD11, 1 h/80°C were used. DMSO gave the best results in terms of conversion with a value of 47.6% and enantioselectivity with an *ee* value of 83.18% in favor to the less active *R*-enantiomer (Table 2).

3.5. Structural studies

3.5.1. Three-dimensional structure of EstD11

The crystal structure of EstD11 was solved at atomic resolution (1.2 Å) (Fig. 6A) yielding high-quality electron density maps that cover nearly the complete EstD11 sequence (residues 2–296) (Fig. S5). Two monomers are present in the asymmetric unit of the crystal with identical structure (RMSD of 0.175 Å for the superposition of 217 Cα atoms). EstD11 presents an α/β hydrolase fold (IPR029058) from superfamily 3 (Fig. S6) as predicted by InterPro [63]. Within this superfamily, EstD11 would belong to the IV-GDSAGG HSL family according to the α/β- hydrolase fold enzyme family 3DM database [2].

Based on structural superimposition with other HSL family members (see below) the catalytic machinery of EstD11 is carried out by a catalytic triad (Ser144, Glu238, His268) and an oxyanion hole delimited by residues Gly76, Gly77 and Ala145. The oxyanion sequence His-Gly-Gly-Gly (74–77), upstream of the active site, is conserved in the HSL family and it agrees with the classification criteria established in the α/β-hydrolase fold 3DM database [2]. Furthermore, the N-terminal neighbor of the Nucleophile serine is an Aspartic (Asp143), a feature conserved in members of IV subfamily.

The catalytic cavity is covered by a cap domain (Fig. 6B) composed by two subdomains coming from different parts of the sequence. Cap subdomain 1 is located at the N-terminal region (residues 2–43) and cap subdomain 2 is inserted between beta strands β6 and β7 of the α/β hydrolase core (residues 172–225) (Fig. S6).

We detected an unusual high percentage of Methionine residues in the EstD11 sequence (3.74% of the entire sequence). Interestingly, all except one are located in the cap (sub)domains and at the interface of the catalytic site forming cross-linked networks akin of the well-known leucine zipper motifs (Fig. 6B). As detailed below these Methionine residues would play a key role in substrate entry and catalysis. In agreement with this role, several

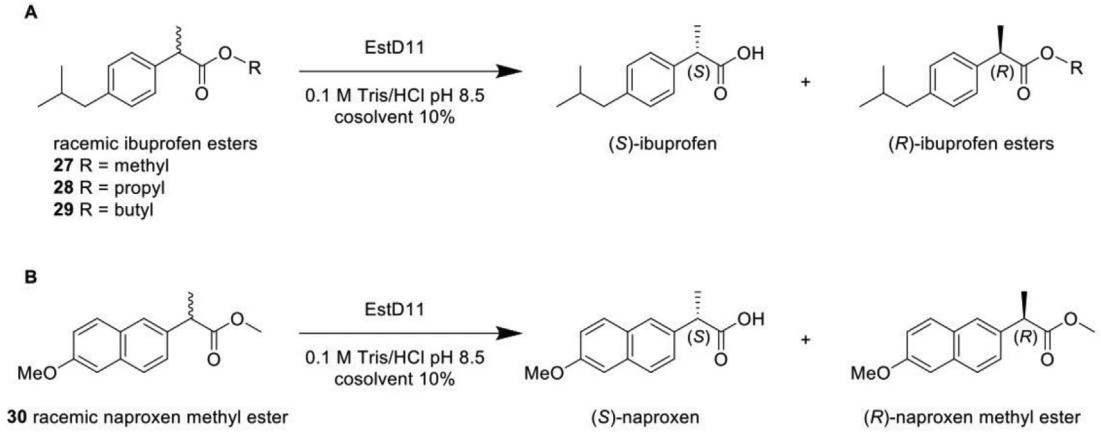

Scheme 2. Reaction conditions used for the resolution of racemic esters of (A) ibuprofen and (B) naproxen.

Table 2
Hydrolysis at 80°C of racemic ibuprofen esters and naproxen methyl ester dissolved in 10% (v/v) DMSO to the *R*-corresponding acids.

Racemic esters	Conversion (%)	*ee* value (%)	*E-value*
27 (ibuprofen methyl ester)	17.95	75.54	n.d.
28 (ibuprofen propyl ester)	15.88	n.d	n.d.
29 (ibuprofen butyl ester)	10.91	89.94	n.d.
30 (naproxen methyl ester)	47.60	83.18	25

n.d.: Not determined. Conditions for the assays: 0.5 U EstD11 (measured with the *p*NP decanoate standard method described in section 2.2.10), 0.136 mmol of racemic esters, 1 h reaction time.

Methionine residues present double rotamer conformations. Not much is known about this disposition of Met residues and just few publications have been reported on the role of Met zipper in dimerization or as substitutes of Leu residues in a Leu zipper [64–66].

Surprisingly, an additional elongated electron density was found inside the substrate pocket in EstD11 for an unknown molecule (Fig. S5B) most likely trapped during the expression or purification processes. The electron density was not compatible with any of the molecules from the crystallization or purification conditions and thus no model was included in the structure. It is worth to mention that something similar happened in an esterase from the same family, PestE from *P. calidifontis* in which an unmodeled density was observed at the acyl binding site region [25].

According to the CATH database [67] closest structural homologues to EstD11 are mesophilic esterases from the same HSL subfamily, EstE5 (PDB:3FAK, RMSD of 0.50 Å for 227 Cα atoms superposition), E40 (PDB: 4XVC, RMSD of 0.53 Å for 232 Cα atoms superposition) and EstE7 (PDB: 3K6K, RMSD of 0.72 Å for 200 Cα atoms superposition) (Fig. S7). As EstD11, all were identified from metagenomic libraries. Interestingly, these structural homologues also have a high percentage content of Met residues localized mainly in cap domain, covering the substrate binding pocket. This structural feature seems to be present in other EstD11 homologues such as EstC23 [45], that also shares similar biochemical behavior (Table S4), for which structure is yet unknown.

3.5.2. Substrate recognition and catalysis in EstD11

In order to gain further insights into substrate recognition and catalysis by EstD11, a series of eight crystallographic complexes were obtained at resolutions ranging from 1.20 to 2.28 Å (Table S3).

An inactive EstD11 mutant (EstD11-S144A) was also produced, crystalized and its structure solved at 1.44 Å resolution (Table S3). As expected, inactive mutant shows an identical structure to that of active enzyme (RMSD of 0.06 Å) and also presented a similar additional unknown electron density at its active site. Cocrystallization of inactive mutant with substrate methyl naproxen (MNP) provided the EstD11-S144A:MNP complex that revealed how the substrate is placed in the catalytic cavity prior to hydrolysis (Fig. 7A). The electron density map for MNP perfectly defines the molecule in one chain (Fig. S8) and in the other the electron density was not of enough quality to model the ligand.

The MNP substrate is located very close to both the catalytic triad and oxyanion hole and mainly stabilized by hydrophobic interactions through Leu31 and Phe273 and also by some Methionine residues from the cap (Met34 and Met193) (Fig. 7A).

In order to get insights into the dynamic of this enzyme at high temperature, EstD11 was incubated with Naproxen *p*NP ester substrate at 30°C for 30 min (see methods), and then crystallized. In this case a new crystal form is produced with just a single chain per asymmetric unit (EstD11:NP complex 1, Table S3). Only the reaction product, naproxen (NP), was observed in the active site (Fig. S8) and, quite surprisingly, four different NP molecules were found attached to the active site (Fig. 7B). The closest naproxen to active site (NP1) establishes polar interactions with Asp143 (one signature motif of the IV subfamily) and with His86; but most of interactions observed for NP1 and the NP products are hydrophobic. The unique discovery of four NP molecules attached to the active site of EstD11, thus far the first evidence of stabilization of multiple products in a HSL structure, provides relevant information on plasticity of this enzyme to allow entry and release of the ligands. Structural comparison of EstD11-S144A:MNP complex and EstD11:NP complex shows that, besides small changes in the disposition of α1, main changes are observed in the loop connecting α1 with α2 (hereafter refer as L1) of sub domain 1 and in the loop connecting α6 with α7 (hereafter refer as L2) of sub domain 2 (Fig. 7B). L1 experiences a strong modification on its conformation with a maximum displacement of 11 Å observed for Cα of Leu19 between the "closed" and "open" forms. The L2 is also affected, showing disorder at the tip of the loop (Ala189). As

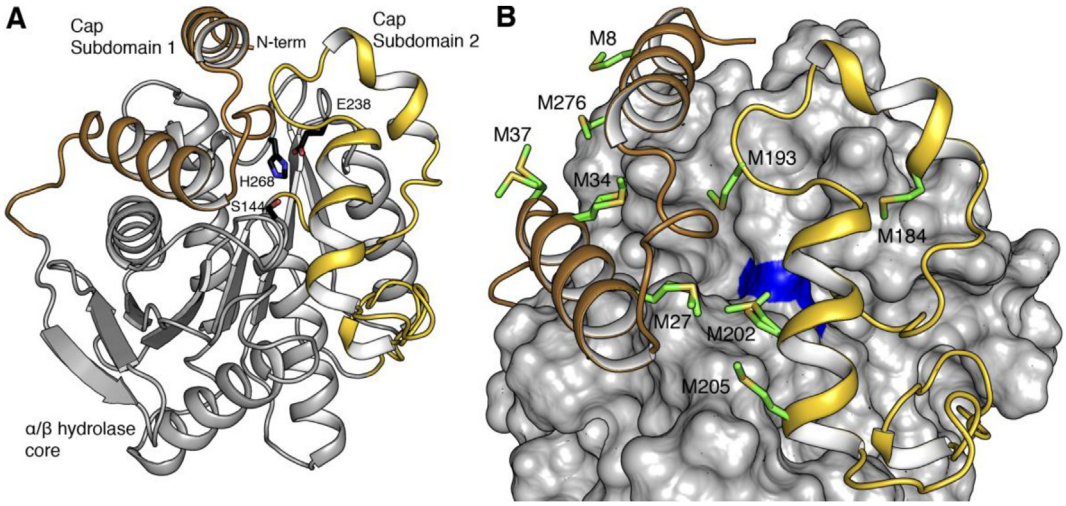

Fig. 6. Three-dimensional structure of EstD11. (A) Cartoon representation of 3D structure of EstD11 with the α/β hydrolase core colored in gray, cap subdomain 1 colored in orange and cap subdomain 2, in yellow. The catalytic triad (Ser144, His268 and Glu238) residues are shown as black capped sticks and labeled. **(B)** Met distribution at the cap domain and at the active site interface. α/β hydrolase core is represented by its molecular surface in gray (position of the catalytic S144 highlighted in dark blue) and cap domains in cartoon. Met residues are drawn as green capped sticks and labeled. (For interpretation of the references to color in this figure legend, the reader is referred to the web version of this article.)

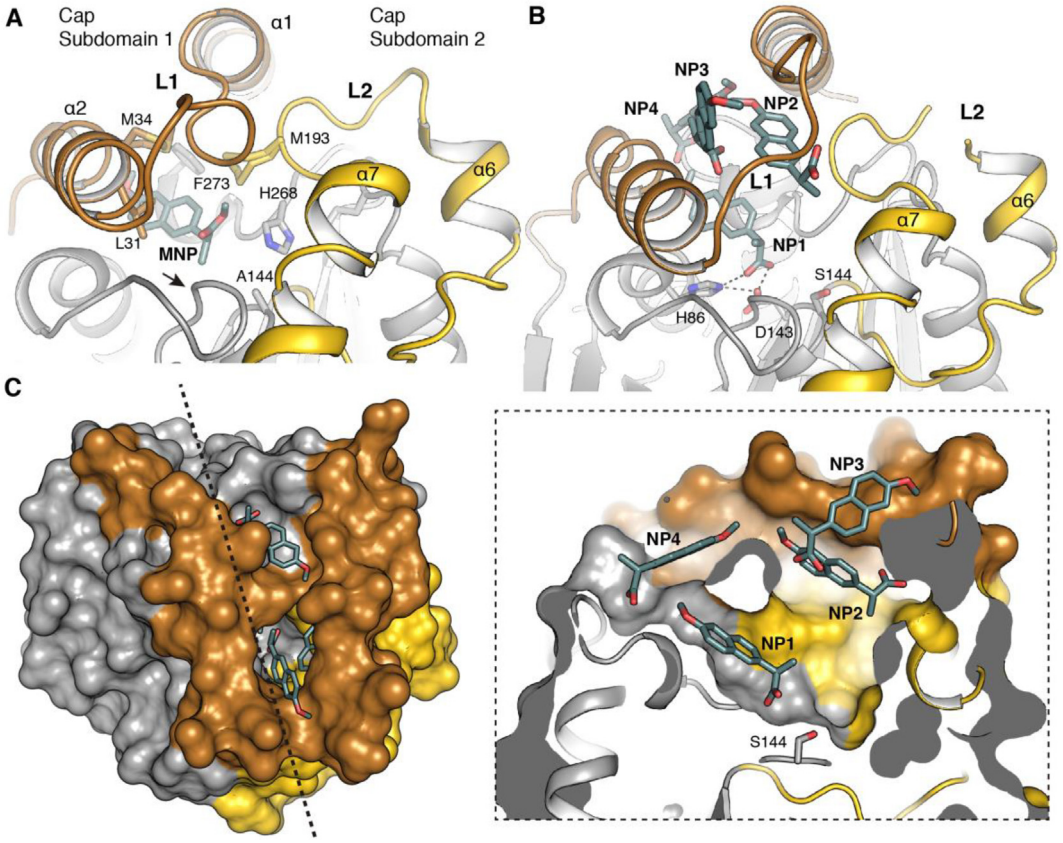

Fig. 7. Naproxen recognition and hydrolysis in EstD11. (A) Methyl naproxen (MNP, represented as green sticks) recognition by inactive EstD11-S144A mutant. Relevant residues are represented as capped sticks and labeled. Loops L1 (connecting α1 with α2) and L2 (connecting α6 with α7) are labeled. Arrow indicates the region with the oxyanion sequence HGGG (74–77). **(B)** Naproxen (NP) products observed after incubation of EstD11 crystals with *p*NP-naproxen at 30°C, prior to crystallization. Up to four molecules where found at the active site of EstD11. The closest naproxen to catalytic Ser144, NP1, is stabilized by polar interactions (dashed lines) with D143 and H86 (labeled). Relevant changes are observed in loops L1 and L2. **(C)** Molecular surface (colored as in Fig. 6) of EstD11:NP complex (left). Naproxen molecules represented as capped sticks. Dotted line represents the section of the view on the right. (For interpretation of the references to color in this figure legend, the reader is referred to the web version of this article.)

detailed below, changes in these loops are of critical relevance for substrate entry and release.

Structural changes in the cap subdomains enlarge the active site cavity and generate tunnels connecting the outer surface of the enzyme with its catalytic site (Fig. 7C).

After the outcomes of the high-temperature crystallographic experiments used for the EstD11:naproxen complex 1, the inactive EstD11-S144A mutant was incubated with naproxen *p*NP ester (NP-*p*NP) substrate under the same high-temperature conditions (see methods). The structure of EstD11-S144A:NP-*p*NP complex (Fig. 8A) was solved at 2.13 Å resolution (Table S3) and presents the complete substrate well defined in the electron density (Fig. S8). The substrate is embraced by the oxyanion residues and it is stabilized mainly by polar interactions concerning the oxygen atoms of the ester bond and involving His86, Asp143 and Gly76, being the last one part of the oxyanion hole. The ester bond of the substrate splits two cavities within the protein, the acyl and alcohol binding sites (Fig. 8B).

The acyl binding site, occupied by the naproxen constituent, is covered by hydrophobic residues, such as Leu13, Leu19, Leu31, Met34, Leu89, Met193, Val269 and Phe273. The double cycle of the substrate is stabilized by hydrophobic contacts as observed in the EstD11-S144A:MNP complex (Fig. 7A). The cavity that tailors the *p*NP group of the substrate, the alcohol binding site, also contains hydrophobic residues (Leu19, Trp174, Val194, Leu199 and Met202) and it is size constrained mainly by the bulky residue Trp174 (Fig. 8B).

3.5.3. Catalytic reaction with pNP-cyclohexane carboxylate and methyl-naproxen. Product stabilization sites in EstD11

Soaking and cocrystallization experiments with the best substrate for EstD11, *p*NP-cyclohexane carboxylate (see methods), resulted in two different complexes with the reaction products cyclohexane carboxylate (CHCA) and *p*NP (Table S3 and Fig. 9A and 9B). Fig. 9C shows the disposition of both products as observed in EstD11:pNP complex 1 and EstD11:CHCA complex.

Furthermore, incubation of wt EstD11 with methyl naproxen resulted in the crystallization of the EstD11:NP complex 2 (Table S3) in which both reaction products, methanol (MOL) and naproxen (NP), are observed in the active site (Fig. 9D).

These three complexes, EstD11:CHCA complex, EstD11:*p*NP complex and EstD11:NP complex 2, provided evidences on location of the acidic and alcohol products from the esterase reaction.

The place occupied by the *p*NP group inside the cavity of the EstD11:*p*NP complex (Fig. 9A) is delimited by L1, L2, α7, loop β3-α3, loop β5- α5, loop β6- α6, loop α6- α7, loop β7- α8 and it is formed by hydrophobic residues. Also, the alcohol product site stabilizing the methanol molecule in EstD11:NP complex 2 (Fig. 9D) overlaps the latter site described in Figs. 8 and 9A.

The site for the acyl product in the EstD11:CHCA structure (Fig. 9B) coincides with the acyl binding site stated above and it is built mainly by hydrophobic amino acids. The catalytic serine lies at the bottom of a tunnel defined by these hydrophobic residues, of approximately 20 Å-length, involving *α1, α2, α3* and helix G2 (Fig. S6). Positions of the acyl products in EstD11:CHCA com-

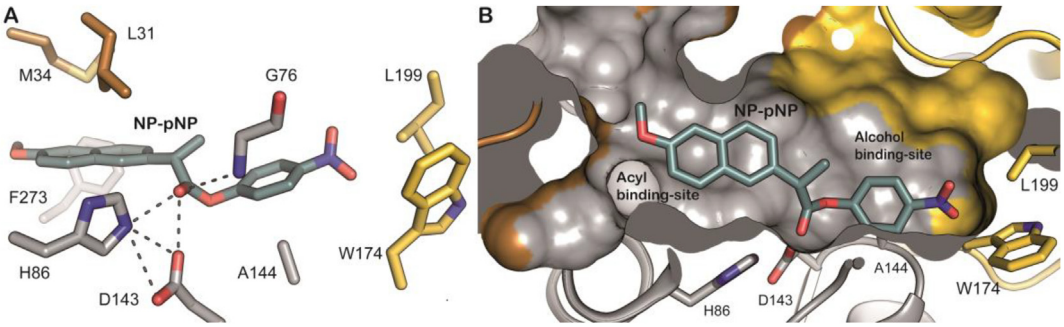

Fig. 8. Acyl and alcohol binding sites in EstD11. EstD11 S144A:naproxen-*p*NP complex. Color scheme used is the same as in Figs. 6 and 7. Key residues are represented in sticks and labelled. NP-*p*NP substrate is represented in green sticks. **(A)** Stabilization of NP-*p*NP substrate by EstD11-S144A mutant. **(B)** Surface representation of EstD11-S144A:nNP-*p*NP complex. Acyl and alcohol binding sites are delimited. (For interpretation of the references to color in this figure legend, the reader is referred to the web version of this article.)

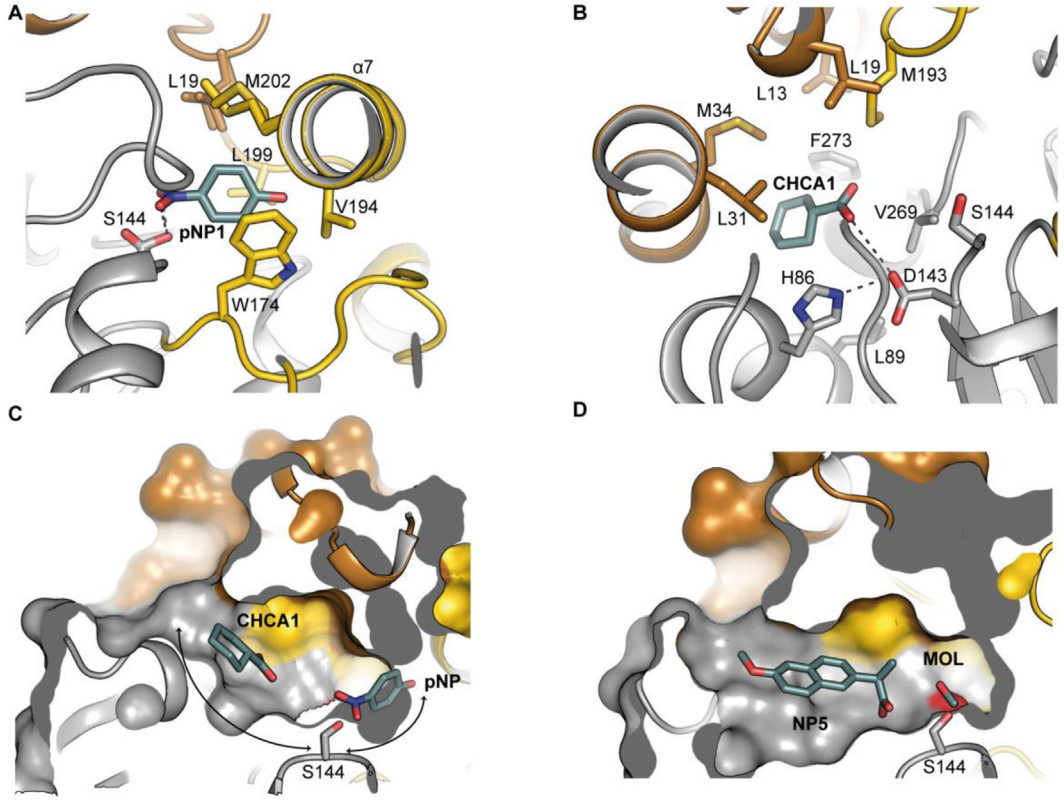

Fig. 9. Products of the catalytic activity of EstD11. Color scheme as in Figs. 6 and 7. **(A)** Stabilization of *p*NP, alcohol product. Key residues are represented in sticks and labelled. Catalytic serine, S144, presents a double conformation and it is interacting with the *p*NP nitro-group. **(B)** Stabilization of CHCA acyl product is mainly done by hydrophobic residues (labelled). The carboxyl group of CHCA1 interacts with Asp143. **(C)** Substrate cavity, superimposition of CHCA and *p*NP complexes, represented in surface. Ligands and Ser144 are represented in sticks. **(D)** Substrate cavity defined in EstD11:NP complex 2.

plex are conserved in EstD11:NP complex 1 (for NP1 and NP4 products) (Fig. 7) and EstD11:NP complex 2 (for NP5 and NP6 products) (Fig. 9D).

3.5.4. Structural characterization of dynamic behavior of cap domains

In order to explore the plasticity of cap subdomains in stabilization and entry of larger substrates, crystallization studies were performed with fluorescein (FLU), a molecule we used for biochemical studies of EstD11 selectivity. Two different EstD11:FLU complexes were obtained as the outcome of different crystal soaking conditions in which different concentrations of fluorescein and incubation times were used (see methods). In both cases, incubation at 30°C was required to get the complexes (see methods).

In the FLU complex 2, solved at 1.97 Å resolution (Table S3), three fluorescein molecules are located on EstD11 surface packed at the interface between the two molecules of the asymmetric unit of the crystal (FLU5-7) (Fig. S9) and another one (FLU8) is located facing the L1 loop and close to the active site entry (Fig. 10C). The second complex, FLU complex 1, solved at 2.28 Å resolution (Table S3), contains fluorescein molecules inside the EstD11 active site. Structural differences are observed among the two independent macromolecules of this crystal. Chain A presents a single FLU molecule (FLU3) inside the catalytic cavity (Fig. 10D). In this case L1 shows a displacement similar to the one observed in the EstD11:NP structure (Fig. 10B) but also notable differences are observed in the cap subdomain 2, for which the high mobility of

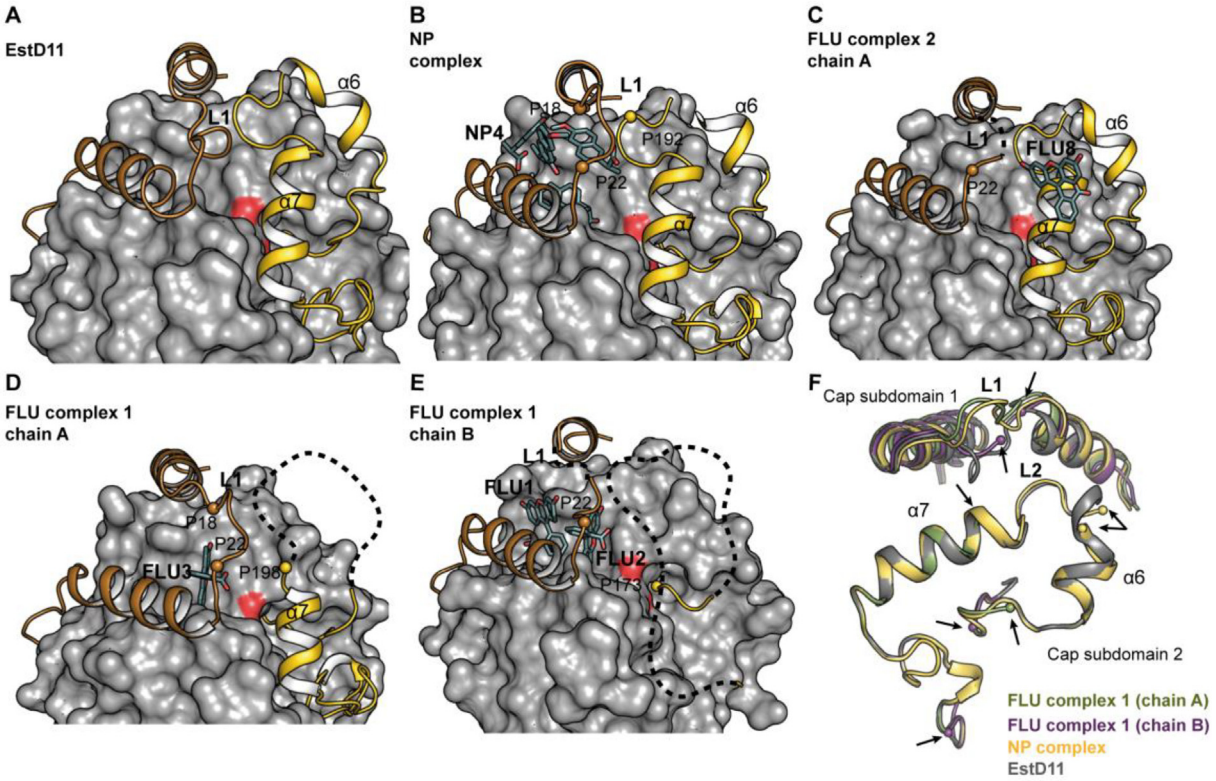

Fig. 10. EstD11 cap domain dynamics. Catalytic domain is represented in gray surface and cap domain is represented in cartoon; subdomain 1 colored in orange and subdomain 2 in yellow. Catalytic Ser144 is colored in red. Ligands are represented in sticks and position of relevant Proline residues indicated by spheres and labeled. Disordered regions are represented in dashed lines. **(A)** EstD11 structure. Native disposition of L1 and L2. **(B)** EstD11:NP complex. Strong displacement of L1, delimited by Pro18 and Pro22, and light mobility shown in L2. Pro192 is maintaining cap domain structure. **(C)** EstD11:FLU (complex 2). A molecule of fluorescein (FLU8) is facing the L1 that is partially disordered. L2 remains unaltered. **(D)** EstD11:FLU chain A (complex 1). L1 experiences a displacement similar to the one observed in EstD11:NP complex. Cap subdomain 2 presents mobility in α6. α7 structure remains unaltered after Pro198. **(E)** EstD11:FLU chainB (complex 1). L1 is displaced and strong changes are observed in cap subdomain 2, upon the presence of two FLU molecules in the substrate cavity. **(F)** Cap domain superimposition. EstD11 structure is represented in gray, NP complex, in yellow, FLU complex 1 (chain A), in green, and FLU complex 1 (chain B), in purple. Limits of the visible regions in the cap subdomains 1 and 2 are indicated by spheres and highlighted by arrows. (For interpretation of the references to color in this figure legend, the reader is referred to the web version of this article.)

L2, α6 and part of α7 precludes its modelling into the electron density map (Fig. 10D). Chain B, presents two FLU molecules (FLU1 and FLU2) inside the active site (Fig. 10E) resulting in a both partially disordered L1 loop and complete disorder in the whole cap subdomain 2, making this zone invisible into the electron density map (Fig. 10E). Thus, the here reported ensemble of complexes provides a structural description (Fig. 10F) of the plasticity of cap subdomains 1 and 2 allowing entry of quite different substrates.

Interestingly, Proline residues were identified delimiting the mobile zones: Pro173 is located in the loop connecting cap subdomain 2 with the catalytic core, Pro192 is located prior to α7 and Pro198, inside this α7 helix. Also, the same occurs in L1, with Pro18 and Pro22 acting as hinges holding the overall structure.

4. Discussion

In this study a metagenomic library constructed from hot spring water DNA was screened for lipolytic activity and the gen was identified. The new esterase, EstD11, was cloned in *E coli*, overexpressed, purified and crystallized. EstD11 was found to belong to the HSL family from the superfamily of α/β-hydrolases.

EstD11 presents a clear thermophilic character with an optimal reaction temperature of 60°C and excellent thermostability by keeping high activity for more than four hours at 70°C, temperature slightly higher than the T_m value of the protein determined by DSF. EstD11 was also stable in the presence of several organic solvents frequently used in biocatalysis. Several thermophilic carboxylesterases from the HSL family have been reported to exist in dimeric, trimeric or higher associations and the oligomeric state being responsible for their high stability [24,25]. By contrast, others, as EstD11 is monomeric in solution as determined in this work by SEC experiments.

It has been reported that interdomain hydrophobic interactions can modulate the thermostability in the HSL family [22]. Structural analysis of E40, an HSL esterase from a marine sedimental metagenomic library, revealed that this thermolabile mesophilic enzyme, showing an optimal temperature of 40°C, can improve thermostability by mutating residues in L1 loop by bulky hydrophobic residues [22]. Hydrophobic interactions through bulky residues (Trp, Tyr) typically occur between L1 and α7 regions of thermophilic members of HSL family such as Est2 (Fig. 11). Authors concluded that these hydrophobic interactions are key for the thermostability of microbial HSLs [22]. Structural analysis reveals that, while keeping conserved polar interactions connecting α2 with the αβ hydrolase core (involving Arg28, Glu111, Ala109 and Val79), EstD11 lacks bulky hydrophobic residues at the L1 /α 7 interface (Fig. 11C). Instead Arg201 in α 7 stablishes H-bond interactions with main-chain atoms of L1 (Fig. 11C). Interestingly, a Met zipper is observed linking cap subdomain 1 (Met27, Met34, Leu19, Leu13) with α 7 (Met193, Met202, Met205) that results in a similar conformation for L1 loop to that observed in other thermophilic esterases (Fig. 11D).

Besides thermostability, Met residues seem to play a relevant role in substrate stabilization in EstD11. Flexibility and large con-

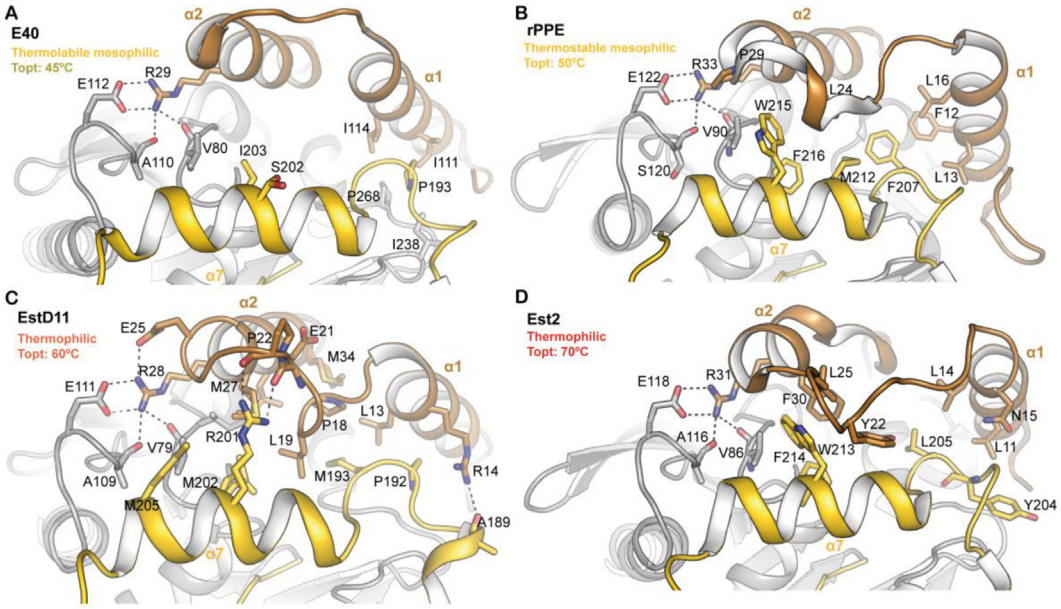

Fig. 11. Structural determinants of EstD11 thermophilic behavior. Analysis of the interactions between cap-subdomain 1 (loop α1-α2) and cap-subdomain 2 in EstD11 and the HSLs homologues: the thermolabile mesophilic E40 (PDB code: 4XVC) from a marine sedimental metagenomic library, the thermostable mesophilic rPPE from *Pseudomonas putida* (PDB code: 4OB8) and the thermophilic Est2 from *Alicyclobacillus acidocaldarius* (PDB code: 1EVQ). The color scheme is the same as in Fig. 6. Key residues are represented in sticks. Optimum temperature (Topt) of EstD11, indicated in colored labels, is in the midst of the rPPE and Est2 HSLs homologues. **(A)** Analysis of cap intradomain interactions in E40. **(B)** A close up on the same region of rPPE. **(C)** EstD11 intradomain stabilization, mainly comprised by hydrophobic interactions mediated by a Methionine zipper. Also, polar residues are present in place of key hydrophobic residues found in Est2 and rPPE (such as R201 instead of W213 in Est2), stabilizing those regions also by polar interactions. (**D**) Est2 interactions, dominated by hydrophobic residues (F214, W213 and F30) [22]. Figure based on Fig. 6 of [22].

formational spectrum of Met residues allow accommodation of different kind of substrates. The EstD11 complexes reveal that side chains of Met both shape the tunnels connecting active site with the outer surface and provide van der Waals contacts with both substrate and reaction products; e.g. in the EstD11:NP complex all the NP molecules are in direct contact with side chain of Met residues. In agreement with this plasticity, many of the Met residues in EstD11 exhibited a double conformation in our crystal structures.

To allow substrates to reach the catalytic site, cap subdomains must move. The different structures of EstD11 in complex with naproxen and fluorescein ligands, reached upon protein incubation and/or crystal soaking at 30°C, provide unique insights on this dynamic (Fig. 10). Incubation of inactive EstD11-S144A with MNP or NP-*p*NP resulted in a single molecule attached to the active site providing information about specific location of the acyl and alcohol binding sites for EstD11 (Fig. 7A). Increasing the incubation temperature of EstD11 with Naproxen *p*NP ester leaded to strong occupancy of naproxen molecules into the active site cavity (Fig. 7B). An 11 Å movement of L1, bounded by Pro18 and Pro22, is observed in this case (Fig. 10B and 10F). Interestingly, when larger substrates, such as fluorescein, are used in these conditions we observe that entrance of a single fluorescein into the active site involves both the observed movement in L1 and also strong disorder in L2 region that loses α6 and part of α7 (Fig. 10D). When two fluorescein molecules enter into the active site, disorder is then observed in both L1 and in the complete cap subdomain 2 (Fig. 10E). It is worth to mention that in all these cases Pro residues bound the amplitude of the movement (Fig. 10). Thus, characterization of movements in cap subdomains together with identification of the sequential disordered events obtained in the variety of EstD11structures could represent snapshots of the dynamic during EstD11 catalytic process.

Incidentally, our structures in complex with fluorescein may rationalize the high fluorescence obtained in the DSF experiment at low temperatures (40°C) as (i) some of them bound exposed hydrophobic patches (as observed in chain B of complex EstD11:FLU complex 2, Fig. S9) and (ii) the entrance of fluorescein into the catalytic site of EstD11 induces strong mobility of cap subdomain 2 exposing large hydrophobic patches (Fig. S9B) that can be target of the hydrophobic dye used in our experiments.

The activity and enantioselectivity of EstD11 was studied towards two esters of chiral carboxylic acids (naproxen and ibuprofen; Scheme 2) as representative substrates. EstD11 showed high activity, and *R*-enantiopreference towards both carboxylic acids.

Based on molecular dynamics and automated docking calculations it has been proposed [25] that the processive orientation of the substrate in the active site of esterase PestE is always with the carboxylic acid side binding in channel 1, and two of the substituents of the carbon of a chiral alcohol binding in channel 2 (alcohol binding site) and the binding pocket (Fig. 12A).

Cavity calculation by using CAVER [68] revealed a different distribution of tunnels in EstD11 (Fig. 12B). Structural comparison of these tunnels with the binding pockets observed in the EstD11 S144A:NP-*p*NP complex, reveals channel 1 corresponds to the alcohol binding site, while the so-called binding pocket will act as the acyl binding site.

EstD11 cavities' distribution, different to that seen in PestE, is similar to the one observed for Est2Aa M211S/ R215L [69].

Channel 2 and binding pocket are roughly preserved in both PestE and EstD11 structures, channel 1 is oriented in a different way in the two esterases. Presence of Trp174 and Leu199 in EstD11 (Ala187 and Met214 in PestE) blocks channel 1 as observed in PestE and keeps a very narrow cavity in channel 1 in the region close to catalytic Ser (5.5 Å from Ser144 to Trp174) (Fig. 12A and 12B). Overall thickening for both channel 1 and 2 is observed upon substrate binding as occurs in EstD11:NP complex 1 (Fig. 12C); however, the cavity is very narrow between the catalytic Ser and Trp174. It is worth to mention that, while Trp174 keeps the same

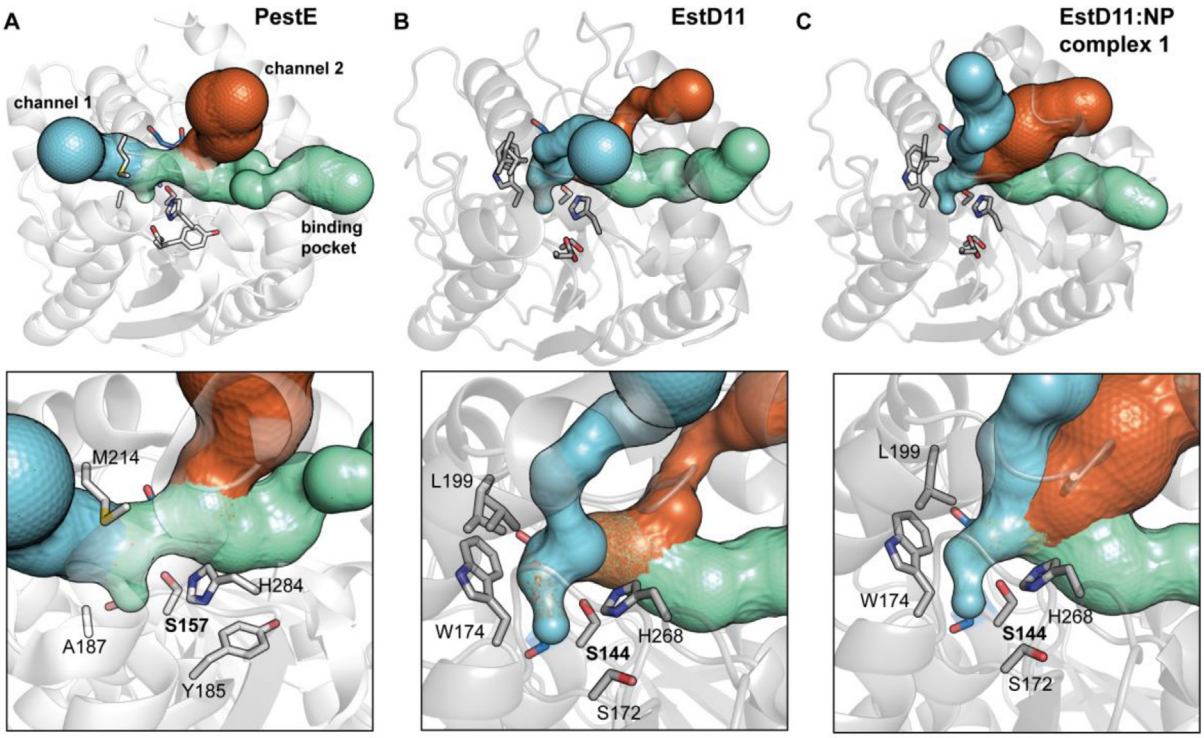

Fig. 12. Comparison of surfaces of the access channels to the active site between the HSL esterases PestE (PDB code:3ZWQ) and EstD11. Protein structures are represented in transparent cartoon and key residues are shown in sticks. Surfaces were calculated by using Caver 3.0 [68]. **(A)** PestE structure. Identification of the cavities, channel 1, channel 2 and binding pocket, is based on [25]. The color scheme, blue for channel 1, orange for channel 2 and green for the binding pocket, is maintained as a reference for Figures B and C. **(B)** EstD11 structure. Distribution and location of the channels varies in relation with PestE. Channel 1, identified for the previous esterase, is blocked by Trp174 and Leu199 while PestE presents an alanine (Ala187) and a methionine (Met213) instead. **(C)** In EstD11:NP complex 1, the cavities become enlarged embracing the naproxen molecules. (For interpretation of the references to color in this figure legend, the reader is referred to the web version of this article.)

conformation among the different EstD11 structures, Leu199 change its conformation depending on the ligand bound to the active site.

The presence of these two residues seems to be important in the overall conformation of channel 1 in EstD11, thus we compared presence of a Trp residue, or an analogous bulky hydrophobic residue, in structural homologues (Table S5). While closest structural homologues of EstD11 (E40 PDB 4XVC, EstE5 PDB 3FAK, EstE7 PDB 3K6K) keep a Trp or a bulky hydrophobic residue at this position, others such as PestE (PDB 3ZWQ), Est2 Aa (PDB 1EVQ) or AFEST (PDB 1JJI) present a short-chain residue (Ala, Ser, Val) (Table S5). It has been reported that the presence of an aromatic residue at position 185 (Tyr185 in PestE, Fig. 12A) close to the catalytic Ser affects substrate recognition in HSL members [49]. Interestingly, this aromatic residue is conserved in the HSL group lacking the Trp residue at position 174 (EstD11 numbering). Conversely, those enzymes from the EstD11 group having such Trp residue, show a Ser residue (Ser172 in EstD11, Fig. 12B) instead of an aromatic residue. In agreement, these two groups have different substrate specificity; while enzymes containing a bulky aromatic residue at position 174 (EstD11 numbering) have preference for short chain ester compounds (C4-C10) with the highest activity towards *p*NPC4 [25,50], those lacking this bulky residue but presenting an aromatic residue at position 185 (PestE numbering) show preference for relatively larger substrates (Est2, optimally hydrolyzes esters with an acyl chain length of 6–8 carbon atoms [52]). It is also worth to mention that enzymes from EstD11 group have considerable catalytic activity against a broad length range of substrates (C2-C16) and they all contain a high percentage of Met residues, while PestE group do not. In this manner, we could short the HSL members analyzed in two groups presenting specific structural features.

As detailed before, in EstD11 we have observed that activity on *p*NP benzoate was nearly zero but increasing the length of the linker between the ester bond and the benzyl ring by, three, or four methylene groups, largely increased catalytic activity. This result would agree with the observed narrow channel 1 in EstD11, that would limit the activity to flexible ligands capable to accommodate into the specific conformation of this channel. In the same line, the steric hindrance and increased volume imposed by linkers with α- or β-methyl groups relative to the ester bond of substrates **26** and **25**, would likely found restrictions to fit channel 1, which would account for the drop in EstD11 activity over these substrates in comparison to the activity on linear aliphatic *p*NP esters of similar chain length (**17**).

Comparison of catalytic efficiency values across a full range of *p*NP esters revealed the broad substrate specificity of EstD11 with significant measurable activity against 16 substrates with varied chain length, steric hindrance or aromaticity. Activity was greatly dependent on aromaticity and flexibility in the ring attachment. Cyclohexyl rings appended to the ester bond were hydrolyzed by EstD11 if they were aliphatic but not the aromatic ones unless a non-branched aliphatic linker is introduced between the aromatic ring and the ester bond. Thus, the far best substrate for EstD11 was on *p*NP cyclohexanecarboxylate. Other bacterial hydrolases have shown minimal activity toward cycloalkyl substrates [57,58] and those that do hydrolyze them, as FTT0941c esterase from *F. tularensis*, do not greatly favor the substrate with the nonaromatic ring (**12**) over the aromatic (**1**), as EstD11 does, indicating a high degree of selectivity for this substrate [13,34,35]. This ability might

be connected to metabolic pathways required for growth under opportunistic metabolic conditions [59].

Amongst the aliphatic *p*NP esters, EstD11 showed clear preference for short-chain ones (C4) with activity decaying as the acyl chain length increased (unsaturated or not), perfectly matching with the substrate selectivity determined for the fluorescein diester substrates. Indeed k_{cat}/K_M values for EstD11 were one order of magnitude higher for FdC6 than for the derivatives with acyl chains 8 or 12C atoms long. EstD11 preference for short-chain esters resembles other enzymes identify from metagenomic libraries after screening on tributyrin-containing plates [18,54,61,62].

Structural and biochemical characterization of EstD11 provides unique information about both activity for this class of enzymes and the molecular basis for its behavior. Considering the identification, here reported, of a group of esterases sharing similar structural and functional features with EstD11; our work paves the way for rational design of new esterases with improved capacities against biotechnologically or biomedically relevant compounds.

Author contribution

Vega Miguel-Ruano: Data curation, Investigation, Methodology, Writing - review & editing. **Ivanna Rivera:** Data curation, Investigation, Writing - review & editing. **Jelena Rajkovic:** Data curation, Investigation, Methodology, Writing - review & editing. **Kamila Knapik:** Data curation, Investigation, Methodology, Writing - review & editing. **Ana Torrado:** Data curation, Investigation, Writing - review & editing. **José Manuel Otero:** Data curation, Investigation, Methodology, Writing - review & editing. **Elisa Beneventi:** Data curation, Investigation, Methodology, Writing - review & editing. **Manuel Becerra:** Data curation, Investigation, Writing - review & editing. **Mercedes Sánchez-Costa:** Data curation, Investigation, Writing - review & editing. **Aurelio Hidalgo:** Data curation, Methodology, Writing - review & editing. **José Berenguer:** Funding acquisition, Methodology, Supervision, Writing - review & editing. **María-Isabel González-Siso:** Conceptualization, Data curation, Methodology, Supervision, Writing - review & editing. **Jacobo Cruces:** Methodology, Supervision, Writing - review & editing. **María L. Rúa:** Conceptualization, Data curation, Methodology, Supervision, Writing - original draft, Writing - review & editing. **Juan A. Hermoso:** Conceptualization, Data curation, Funding acquisition, Methodology, Supervision, Writing - original draft, Writing - review & editing.

Declaration of Competing Interest

The authors declare that they have no known competing financial interests or personal relationships that could have appeared to influence the work reported in this paper.

Acknowledgments

We thank the staff from ALBA synchrotron facility (Barcelona, Spain) for support during crystallographic data collection. This work was funded by the UE through the HotDrops Project (FP7-PEOPLE-2012-IAPP, project number 324439). Additionally, this work was supported by the BFU2017-90030-P grant to J.A.H. from the Spanish Ministry of Science and Innovation.

Appendix A. Supplementary data

Supplementary data to this article can be found online at https://doi.org/10.1016/j.csbj.2021.01.047.

References

[1] Ollis DL, Cheah E, Cygler M, Dijkstra B, Frolow F, Franken SM, et al. The α/β hydrolase fold. Protein Eng 1992;5:197–211.
[2] Kourist R, Jochens H, Bartsch S, Kuipers R, Padhi SK, Gall M, et al. The α/β-hydrolase fold 3DM database (ABHDB) as a tool for protein engineering. ChemBioChem 2010;11:1635–43. https://doi.org/10.1002/cbic.201000213.
[3] Fojan P, Jonson PH, Petersen MTN, Petersen SB. What distinguishes an esterase from a lipase: A novel structural approach. Biochimie 2000;82:1033–41.
[4] H.M. Tahir R.N.Z.R.A. Rahman A.T.C. Leow M.S.M. Ali Expression, characterisation and homology modelling of a novel hormone-sensitive lipase (HSL)-like esterase from Glaciozyma antarctica Catalysts 2020;10:1–19. 10.3390/catal10010058
[5] Bornscheuer UT, Kazlauskas RJ. Hydrolases in organic synthesis: regio- and stereoselective biotransformations: Second Edition. Wiley-VCH Verlag GmbH & Co. KGaA; 2006. Doi: 10.1002/3527607544.
[6] Kim TD. Bacterial hormone-sensitive lipases (bHSLs): Emerging enzymes for biotechnological applications. J Microbiol Biotechnol 2017;27:1907–15. https://doi.org/10.4014/jmb.1708.08004.
[7] Müller H, Becker AK, Palm GJ, Berndt L, Badenhorst CPS, Godehard SP, et al. Sequence-based prediction of promiscuous acyltransferase activity in hydrolases. Angew Chem Int Ed 2020;59:11607–12. https://doi.org/10.1002/anie.202003635.
[8] Ferrer M, Bargiela R, Martínez-Martínez M, Mir J, Koch R, Golyshina O, et al. Biodiversity for biocatalysis: A review of the α/β-hydrolase fold superfamily of esterases-lipases discovered in metagenomes. Biocatal Biotransformation 2015;33:235–49. https://doi.org/10.3109/10242422.2016.1151416.
[9] Neugnot V, Moulin G, Dubreucq E, Bigey F. The lipase/acyltransferase from Candida parapsilosis: Molecular cloning and characterization of purified recombinant enzymes. Eur J Biochem 2002;269:1734–45. https://doi.org/10.1046/j.1432-1327.2002.02828.x.
[10] Samoylova Y, Sorokina K, Piligaev A, Parmon V. Application of bacterial thermostable lipolytic enzymes in the modern biotechnological processes: A Review. Catal Ind 2019;11:168–78. https://doi.org/10.1134/S2070050419020107.
[11] Martínez-Martínez M, Coscolín C, Santiago G, Chow J, Stogios PJ, Bargiela R, et al. Determinants and prediction of esterase substrate promiscuity patterns. ACS Chem Biol 2018;13:225–34. https://doi.org/10.1021/acschembio.7b00996.
[12] Arpigny J, Jaeger K. Bacterial lipolytic enzymes: classification and properties. Biochem J 1999;343:177–83. https://doi.org/10.1042/bj3430177.
[13] López-López O, Cerdán ME, Gonzalez-Siso MI. New extremophilic lipases and esterases from metagenomics. Curr Prot Pept Sci 2014;15:445–55. https://doi.org/10.2174/1389203715666140228153801.
[14] Kovacic F, Babic N, Krauss U, Jaeger K. Classification of lipolytic enzymes from bacteria. Aerobic utilization of hydrocarbons, oils, and lipids, Cham: Springer International Publishing; 2019, p. 255–89. Doi: 10.1007/978-3-319-50418-6_39.
[15] Hitch TCA, Clavel T. A proposed update for the classification and description of bacterial lipolytic enzymes. PeerJ 2019;7:e7249-undefined. Doi: 10.7717/peerj.7249.
[16] Bornscheuer UT. Microbial carboxyl esterases: Classification, properties and application in biocatalysis. FEMS Microbiol Rev 2002;26:73–81. https://doi.org/10.1016/S0168-6445(01)00075-4.
[17] Jeon JH, Lee HS, Kim JT, Kim SJ, Choi SH, Kang SG, et al. Identification of a new subfamily of salt-tolerant esterases from a metagenomic library of tidal flat sediment. Appl Microbiol Biotechnol 2012;93:623–31. https://doi.org/10.1007/s00253-011-3433-x.
[18] Li P, Ji P, Li C, Zhang Y, Wang G, Zhang X, et al. Structural basis for dimerization and catalysis of a novel esterase from the GTSAG motif subfamily of the bacterial hormone-sensitive lipase family. J Biol Chem 2014;289:19031–41. https://doi.org/10.1074/jbc.M114.574913.
[19] Boyko KM, Kryukova M v., Petrovskaya LE, Nikolaeva AY, Korzhenevsky DA, Novototskaya-Vlasova KA, et al. Crystal structure of PMGL2 esterase from the hormone-sensitive lipase family with GCSAG motif around the catalytic serine. PLoS ONE 2020;15:1–15. Doi: 10.1371/journal.pone.0226838.
[20] Kryukova M, Petrovskaya L, Novototskaya-Vlasova K, Kryukova E, Yakimov S, Nikolaeva A, et al. Effect of cysteine residue substitution in the GCSAG motif of the PMGL2 esterase active site on the enzyme properties. Biochem 2020;85:709–16. https://doi.org/10.1134/S0006297920060085.
[21] Huang J, Huo Y, Ji R, Kuang S, Ji C, Xu X, et al. Structural insights of a hormone sensitive lipase homologue Est22. Sci Rep 2016;6:28550-undefined. Doi: 10.1038/srep28550.
[22] Li P, Chen X, Ji P, Li C, Wang P, Zhang Y, et al. Interdomain hydrophobic interactions modulate the thermostability of microbial esterases from the hormone-sensitive lipase family. J Biol Chem 2015;290:11188–98. https://doi.org/10.1074/jbc.M115.646182.
[23] Wei Y, Contreras JA, Sheffield P, Osterlund T, Derewenda U, Kneusel RE, et al. Crystal structure of brefeldin a esterase, a bacterial homolog of the mammalian hormonesensitive lipase. Nat Struct Biol 1999;6:340–5. https://doi.org/10.1038/7576.
[24] Angkawidjaja C, Koga Y, Takano K, Kanaya S. Structure and stability of a thermostable carboxylesterase from the thermoacidophilic archaeon Sulfolobus tokodaii. FEBS J 2012;279:3071–84. https://doi.org/10.1111/j.1742-4658.2012.08687.x.

[25] Palm GJ, Fernández-Álvaro E, Bogdanović X, Bartsch S, Sczodrok J, Singh RK, et al. The crystal structure of an esterase from the hyperthermophilic microorganism Pyrobaculum calidifontis VA1 explains its enantioselectivity. Appl Microbiol Biotechnol 2011;91:1061–72. https://doi.org/10.1007/s00253-011-3337-9.
[26] Wohlgemuth R, Littlechild J, Monti D, Schnorr K, van Rossum T, Siebers B, et al. Discovering novel hydrolases from hot environments. Biotechnol Adv 2018;36:2077–100. https://doi.org/10.1016/j.biotechadv.2018.09.004.
[27] Mandrich L, Merone L, Pezzullo M, Cipolla L, Nicotra F, Rossi M, et al. Role of the N terminus in enzyme activity, stability and specificity in thermophilic esterases belonging to the HSL family. J Mol Biol 2005;345:501–12. https://doi.org/10.1016/j.jmb.2004.10.035.
[28] Ferrer M, Martínez-Martínez M, Bargiela R, Streit WR, Golyshina O, Golyshin P. Estimating the success of enzyme bioprospecting through metagenomics: Current status and future trends. Microb Biotechnol 2016;9:22–34. https://doi.org/10.1111/1751-7915.12309.
[29] Petrovskaya L, Novototskaya-Vlasova K, Gapizov S, Spirina E, Durdenko E, Rivkina E. New member of the hormone-sensitive lipase family from the permafrost microbial community. Bioengineered 2017;8:420–3. https://doi.org/10.1080/21655979.2016.1230571.
[30] Angelov A, Mientus M, Liebl S, Liebl W. A two-host fosmid system for functional screening of (meta)genomic libraries from extreme thermophiles. Syst Appl Microbiol 2009;32:177–85. https://doi.org/10.1016/j.syapm.2008.01.003.
[31] Kim YJ, Kim HHS, Kim SH, Rha E, Choi SL, Yeom SJ, et al. Improved metagenome screening efficiency by random insertion of T7 promoters. J Biotechnol 2016;230:47–53. https://doi.org/10.1016/j.jbiotec.2016.05.018.
[32] Ko K, Rim S, Han Y, Shin B, Kim G, Choi J, et al. Identification and characterization of a novel cold-adapted esterase from a metagenomic library of mountain soil. J Ind Microbiol Biotechnol 2012;39:681–9. https://doi.org/10.1007/s10295-011-1080-y.
[33] Okano H, Hong X, Kanaya E, Angkawidjaja C, Kanaya S. Structural and biochemical characterization of a metagenome-derived esterase with a long N-terminal extension. Protein Sci 2015;24:93–104. https://doi.org/10.1002/pro.2591.
[34] Altschul SF, Gish W, Miller W, Myers EW, Lipman DJ. Basic local alignment search tool. J Mol Biol 1990;215:403–10. https://doi.org/10.1016/S0022-2836(05)80360-2.
[35] Sievers F, Higgins DG. Clustal omega, accurate alignment of very large numbers of sequences. Methods Mol Biol 2014;1079:105–16. https://doi.org/10.1007/978-1-62703-646-7_6.
[36] Kumar S, Stecher G, Tamura K, Dudley J. MEGA7: Molecular evolutionary genetics analysis version 7.0 for bigger datasets. Mol Biol Evol 2016;33:1870–4. Doi: 10.1093/molbev/msw054.
[37] Gasteiger E, Hoogland C, Gattiker A, Duvaud S, Wilkins MR, Appel RD, et al. Protein identification and analysis tools on the ExPASy server. In: Walker JM, editor. The Proteomics Protocols Handbook, Humana Press; 2005, p. 571–607.
[38] Fuciños P, Abadín CM, Sanromán A, Longo MA, Pastrana L, Rúa ML. Identification of extracellular lipases/esterases produced by Thermus thermophilus HB27: partial purification and preliminary biochemical characterisation. J Biotechnol 2005;117:233–41.
[39] Kim S, Lee JI, Kim YC. A simple and mild esterification method for carboxylic acids using mixed carboxylic-carbonic anhydrides. J Org Chem 1985;50:560–5. https://doi.org/10.1021/jo00205a004.
[40] Niesen FH, Berglund H, Vedadi M. The use of differential scanning fluorimetry to detect ligand interactions that promote protein stability. Nat Protoc 2007;2:2212–21. https://doi.org/10.1038/nprot.2007.321.
[41] Kabsch W. XDS. Acta Crystallogr D Biol Crystallogr 2010;66:125–32.
[42] Evans PR, Murshudov GN. How good are my data and what is the resolution?. Acta Crystallogr D Biol Crystallogr 2013;69:1204–14. https://doi.org/10.1107/S0907444913000061.
[43] Emsley P, Lohkamp B, Scott WG, Cowtan K. Features and development of Coot. Acta Crystallogr D Biol Crystallogr 2010;66:486–501. https://doi.org/10.1107/S0907444910007493.
[44] Murshudov GN, Skubák P, Lebedev AA, Pannu NS, Steiner RA, Nicholls RA, et al. REFMAC5 for the refinement of macromolecular crystal structures. Acta Crystallogr D Biol Crystallogr 2011;67:355–67. https://doi.org/10.1107/S0907444911001314.
[45] Jin P, Pei X, Du P, Yin X, Xiong X, Wu H, et al. Overexpression and characterization of a new organic solvent-tolerant esterase derived from soil metagenomic DNA. Bioresour Technol 2012;116:234–40. https://doi.org/10.1016/j.biortech.2011.10.087.
[46] Zieniuk B, Fabiszewska A, Białecka-Florjańczyk E. Screening of solvents for favoring hydrolytic activity of Candida antarctica Lipase B. Bioprocess Biosyst Eng 2020;43:605–13. https://doi.org/10.1007/s00449-019-02252-0.
[47] Li C, Tan T, Zhang H, Feng W. Analysis of the conformational stability and activity of Candida antarctica lipase B in organic solvents: Insight from molecular dynamics and quantum mechanics/simulations. J Biol Chem 2010;285:28434–41. https://doi.org/10.1074/jbc.M110.136200.
[48] Lotti M, Pleiss J, Valero F, Ferrer P. Effects of methanol on lipases: Molecular, kinetic and process issues in the production of biodiesel. Biotechnol J 2015;10:22–30. https://doi.org/10.1002/biot.201400158.
[49] Boivin S, Kozak S, Meijers R. Optimization of protein purification and characterization using Thermofluor screens. Protein Expr Purif 2013;91:192–206. https://doi.org/10.1016/j.pep.2013.08.002.
[50] Ericsson UB, Hallberg BM, DeTitta GT, Dekker N, Nordlund P. Thermofluor-based high-throughput stability optimization of proteins for structural studies. Anal Biochem 2006;357:289–98. https://doi.org/10.1016/j.ab.2006.07.027.
[51] Pantoliano MW, Petrella EC, Kwasnoski JD, Lobanov VS, Myslik J, Graf E, et al. High-density miniaturized thermal shift assays as a general strategy for drug discovery. J Biomol Screen 2001;6:429–40. https://doi.org/10.1089/108705701753364922.
[52] Metin K, Ateslier Z, Basbulbul G, Biyik H. Characterization of esterase activity in Geobacillus sp. HBB-4. J Basic Microbiol 2006;46:400–9.
[53] Petrovskaya L, Novototskaya-Vlasova K, Spirina E, Durdenko E, Lomakina G, Zavialova M, et al. Expression and characterization of a new esterase with GCSAG motif from a permafrost metagenomic library. FEMS Microbiol Ecol 2016;92:fiw046-undefined. Doi: 10.1093/femsec/fiw046.
[54] Nagaroor V, Gummadi SN. Biochemical characterization of an esterase from Clostridium acetobutylicum with novel GYSMG pentapeptide motif at the catalytic domain. J Ind Microbiol Biotechnol 2020;47:169–81. https://doi.org/10.1007/s10295-019-02253-8.
[55] Huynh K, Partch CL. Analysis of protein stability and ligand interactions by thermal shift assay. Curr Protoc Protein Sci 2015;79:28.9.1-28.9.14. Doi: 10.1002/0471140864.ps2809s79.
[56] Vaezzadeh M, Sabbaghian M, Yaghmaei P, Ebrahim-Habibi A. Effect of organic solvents on porcine pancreatic lipase thermal aggregation. Protein Pept Lett 2017;24:955–61. https://doi.org/10.2174/0929866524666170724114947.
[57] Lukowski JK, Savas CP, Gehring AM, McKary MG, Adkins CT, Lavis LD, et al. Distinct substrate selectivity of a metabolic hydrolase from Mycobacterium tuberculosis. Biochemistry 2014;53:7386–95. https://doi.org/10.1021/bi501108u.
[58] Ellis EE, Adkins CT, Galovska NM, Lavis LD, Johnson RJ. Decoupled roles for the atypical, bifurcated binding pocket of the ybfF hydrolase. ChemBioChem 2013;14:1134–44. https://doi.org/10.1002/cbic.201300085.
[59] Farberg AM, Hart WK, Johnson RJ. The unusual substrate specificity of a virulence associated serine hydrolase from the highly toxic bacterium, Francisella tularensis. Biochem Biophys Reports 2016;7:415–22. https://doi.org/10.1016/j.bbrep.2016.07.006.
[60] Fiedler F, Hinz H. No intermediate channelling in stepwise hydrolysis of fluorescein di-β-D-galactoside by β-galactosidase. Eur J Biochem 1994;222:75–81. https://doi.org/10.1111/j.1432-1033.1994.tb18843.x.
[61] Zisis T, Freddolino PL, Turunen P, van Teeseling MCFF, Rowan AE, Blank KG. Interfacial activation of Candida antarctica lipase B: Combined evidence from experiment and simulation. Biochemistry 2015;54:5969–79. https://doi.org/10.1021/acs.biochem.5b00586.
[62] Huang Z. Kinetic fluorescence measurement of fluorescein di-β-D-galactoside hydrolysis by β-galactosidase: Intermediate channeling in stepwise catalysis by a free single enzyme. Biochemistry 1991;30:8535–40. https://doi.org/10.1021/bi00099a006.
[63] Mitchell AL, Attwood TK, Babbitt PC, Blum M, Bork P, Bridge A, et al. InterPro in 2019: Improving coverage, classification and access to protein sequence annotations. Nucleic Acids Res 2019;47:D351–60. https://doi.org/10.1093/nar/gky1100.
[64] Kanaan MN, Fu YH, Marzluf GA. The DNA-binding domain of the cys-3 regulatory protein of Neurospora Crassa is bipartite. Biochemistry 1992;31:3197–203. https://doi.org/10.1021/bi00127a022.
[65] Riboldi-Tunnicliffe A, König B, Jessen S, Weiss MS, Rahfeld J, Hacker J, et al. Crystal structure of Mip, a prolylisomerase from Legionella pneumophila. Nat Struct Biol 2001;8:779–83. https://doi.org/10.1038/nsb0901-779.
[66] Li X, Zhang R, Zhang H, He Y, Ji W, Min W, et al. Crystal structure of CCM3, a cerebral cavernous malformation protein critical for vascular integrity. J Biol Chem 2010;285:24099–107. https://doi.org/10.1074/jbc.M110.128470.
[67] Knudsen M, Wiuf C. The CATH database. Hum Genomics 2010;4:207–12. https://doi.org/10.1186/1479-7364-4-3-207.
[68] Chovancova E, Pavelka A, Benes P, Strnad O, Brezovsky J, Kozlikova B, et al. CAVER 3.0: A tool for the analysis of transport pathways in dynamic protein structures. PLoS Comput Biol 2012;8:23–30. Doi: 10.1371/journal.pcbi.1002708.
[69] de Simone G, Mandrich L, Menchise V, Giordano V, Febbraio F, Rossi M, et al. A substrate-induced switch in the reaction mechanism of a thermophilic esterase: Kinetic evidences and structural basis. J Biol Chem 2004;279:6815–23. https://doi.org/10.1074/jbc.M307738200.
[70] Dror A, Shemesh E, Dayan N, Fishman A. Protein engineering by random mutagenesis and structure-guided consensus of Geobacillus stearothermophilus lipase T6 for enhanced stability in methanol. Appl Environ Microbiol 2014;80:1515–27. https://doi.org/10.1128/AEM.03371-13.